2018-04-24

Near-infrared incoherent broadband cavity enhanced absorption spectroscopy (NIR-IBBCEAS) for detection and quantification of major natural gas components

Prakash, Neeraj

UNIVERSITY OF CALGARY

Near-infrared incoherent broadband cavity enhanced absorption spectroscopy (NIR-IBBCEAS) for detection and quantification of major natural gas components

by

Neeraj Prakash

A THESIS

SUBMITTED TO THE FACULTY OF GRADUATE STUDIES

IN PARTIAL FULFILMENT OF THE REQUIREMENTS FOR THE

DEGREE OF MASTER OF SCIENCE

GRADUATE PROGRAM IN MECHANICAL AND MANUFACTURING ENGINEERING

CALGARY, ALBERTA

APRIL, 2018

Abstract

The efforts for reducing carbon emissions by switching from coal to natural gas have created a bigger threat to global warming through natural gas leaks. Apart from the monetary losses, leakage of natural gas releases methane, which can trap more than 80 times as much heat as carbon dioxide. Most often, the leaks are left unmonitored due to the huge cost and clumsy nature of existing leak detection techniques. Hence, this thesis presents the development of a low cost and efficient technique to simultaneously detect and quantify the major hydrocarbons in natural gas and thereby determine the gas composition. The instrument is based on the principle of incoherent broadband cavity enhanced absorption spectroscopy in the near infrared region (1100 to 1250 nm). The performance and detection sensitivities of the prototype were tested, and results showed detection limits much less than 1% of the lower explosion limits (LEL) of the gases.

Preface

This thesis is original, unpublished, independent work by the author, Neeraj Prakash.

Acknowledgments

A great many people have contributed to the successful completion of this thesis. I would like to extend my gratitude to all those people who supported me during my graduate studies and made it a memorable experience that I will cherish forever. First and foremost, I would like to express my sincere gratitude to my advisor Dr. Ke Du, for his generous and continuous support throughout my graduate studies. I would like to thank him for all the valuable and timely advice and guidance without which this thesis would not have been possible. He had been extremely understanding, motivating and patient throughout, which helped in shaping my research skills. Besides my advisor, I would like to thank Dr. Ravi Varma at National Institute of Technology Calicut, India, for sharing his immense knowledge and experience in the field of optics and cavity enhanced techniques and for allowing me to conduct experiments in his applied optics and instrumentation (AOI) lab. I am also indebted to Dr. Claudio Mazzoleni, Michigan Technological University, and Dr. Wolfgang Tittel, University of Calgary, for providing access to their lab facilities to perform initial tests and experiments. I also thank Dr. Seonghwan Kim and Dr. Simon Park, University of Calgary for their generosity in lending some of the optics and gas regulators which helped in building and testing the instrument.

I am grateful to Arun Ramachandran, AOI lab, and my fellow lab mate, Zhenyu Xing for all the thought-provoking and insightful discussions we had. I also appreciate the help extended by Zhenyu and Koorosh Esteki, Physics department, University of Calgary, during the installation of the instrument. I would also like to acknowledge Dustin from the machine shop, University of Calgary, who helped in machining some parts of the instrument at a lightning-fast pace. I thank my other fellow lab mates and graduate office members as well, for all the fun we had in the last two years.

Moving alone to a new city, leaving behind your dear and near ones, can be extremely difficult. However, I was fortunate enough to make a good bunch of friends who made me feel at home in Calgary. I greatly value their friendship and would like to thank each of them for their care, and support in building together some great memories in Calgary. Finally and most importantly, I would like to express my heartfelt gratitude to my parents, family members and friends for their continuous support, love, concern, and strength.

Dedication

I dedicate this thesis to my dearest and loving grandfather, late T. Kumaran Nair, who has always been a role model I would look up to and an inspiration to all his grandchildren.

Table of Contents

Abstract ii
Preface iii
Acknowledgments iv
Dedication vi
Table of Contents vii
List of Figures and Illustrations ix
List of Symbols, Abbreviations and Nomenclature xii

Chapter 1: Introduction 1
1.1 Natural Gas and its importance 1
1.1.1 Distribution of Natural Gas 4
1.1.2 Challenges of Natural Gas Distribution 5
1.2 Contemporary Natural Gas Leak Detection Techniques 7
1.2.1 Non-Optical Techniques 8
1.2.2 Optical Techniques 9
1.3 Motivation for This Thesis 11

Chapter 2: Incoherent Broadband Cavity Enhanced Absorption Spectroscopy 13
2.1 Absorption Spectroscopy 13
2.2 Principle of IBBCEAS 16
2.3 NIR-IBBCEAS for Natural Gas Detection - Present work 21
2.3.1 Component Details 23

Chapter 3: Initial Testing and Calibration 25
3.1 Qualitative Testing 25
3.1.1 Conclusion 28
3.2 Spectrometer Calibration 29
3.2.1 Spectrometer Resolution 29
3.2.2 Wavelength Calibration 31
3.3 Reference Cross-section Generation 32
3.3.1 Reflectivity Calibration 34
3.3.2 Absorption Cross-section Measurements 37
3.4 Summary 38

Chapter 4: NIR-IBBCEAS Instrumentation 40
4.1 Instrument Set-up 40
4.1.1 Structural Design 41
4.1.2 Light Source 43
4.1.3 Instrument Assembly and Cavity Alignment 45
4.2 Instrument Stability and Allan Variance 49
4.3 Software Development 51
4.4 Summary 54

Chapter 5: Experiments and Analysis 55
5.1 Reflectivity Calibration 55

5.2 Data Analysis **57**
5.2.1 Spectral Fitting **57**
5.2.2 Error Analysis **60**
5.3 Instrument Testing **62**
5.3.1 995.1 ppm Methane sample **63**
5.3.1.1 Signal to Noise Ratio ***64***
5.3.1.2 Detection limit ***64***
5.3.2 Hydrocarbon Mixture **66**

Chapter 6: Conclusion **68**
6.1 Summary of Findings **68**
6.2 Key Highlights **69**
6.3 Assumptions and Limitations **71**
6.4 Future Work **71**

References **74**

Appendix **82**
NIR-IBBCEAS Mirror Reflectivity **82**
Absorption cross-section **87**
Methane **87**
Butane **92**
Ethane **97**
Propane **102**
Platform Design for Light Source Integration **107**

List of Figures and Illustrations

Figure 1: Review of natural gas leak detection methods. 8

Figure 2: Application of absorption spectroscopy for gas detection (Platt & Stutz, 2008). 14

Figure 3: Schematic of an IBBCEAS system. 1, Incoherent broadband source; 2, focusing lens; 3, filter; 4, iris; 5, high reflective cavity mirrors; 6, pressure gauge; 7, gas inlet; 8, cavity cell; 9, gas outlet; 10, aluminum coated mirror; 11, spectrometer. 16

Figure 4: BBCEAS system set up in EOL, MTU. Here, L denotes 1" lens, CM represents cavity mirror and M denotes aluminum-coated mirror. 25

Figure 5: IBBCEAS set-up installed at EOL for qualitative testing of methane and butane detection. 26

Figure 6: Top graph: PD signal generated by the transmitted light intensity when the cavity was flushed with dry air. A.U., implies arbitrary unit. Bottom graph: Measured absorbance ($\ln(I_0/I)$) of methane and butane using the IBBCEAS set-up. 27

Figure 7: A Gaussian fit to the laser peak centered at 1591.436 nm showing a FWHM of 8.71 nm. 30

Figure 8: A second-order polynomial fit of the wavelengths to the pixels. Data represents the true wavelength of the laser peak and the pixel at which the spectrometer measured it. The fit obtained an absolute error of 0.8 nm for the difference between the true and calibrated wavelength. 31

Figure 9: Schematic diagram of the IBBCEAS set-up for cross-section measurements. 1, Xenon lamp; 2, 2" lens (f=3 cm); 3, 2" lens (f=6 cm); 4, highly reflective cavity mirror; 5, gas inlet; 6, PVC pipe; 7, gas outlet; 8, vacuum bellow; 9, long pass filter (1100nm); 10, short pass filter (1250 nm); 11, 1" focusing lens (f= 6 cm); 12, NIRez Spectrometer; 13, Aluminium mirror; 14, He-Ne laser (red). 33

Figure 10: Convoluted and high resolution HITRAN cross-sections of methane and CO_2. 34

Figure 11: Top curve: A typical I_0 spectrum measured using the Xenon lamp. Bottom curve: Dark spectrum obtained by blocking the source. 35

Figure 12: The experimentally determined reflectivity as a function of wavelength in the 1100-1250 nm range for absorption cross-section measurement experiments. The solid line represents a second-order polynomial fit to the reflectivity values (dotted-line curve). The error bars indicate a one standard deviation of ± 0.00018 (fit uncertainty) from the fit. 36

Figure 13: The reference absorption cross-section of (A) butane (R^2=0.977), (B) ethane (R^2=0.965) and (C) propane (R^2=0.962), determined using the NIR-IBBCEAS instrument. 38

Figure 14: Schematic diagram of the NIR-IBBCEAS instrument. 1, Tungsten-Halogen Light source; 2, 2" lens (f=6 cm); 3,4,13,14 Aluminum-coated mirror; 5, 1" focusing lens (f= 2.5 cm); 6, 2" lens (f=7 cm); 7, 8, highly reflective cavity mirror; 9, long pass filter (1100nm); 10, short pass filter (1250 nm); 11, 1" focusing lens (f= 6 cm); 12, NIRez Spectrometer; 15, Alignment laser. 41

Figure 15: The supporting structural framework for housing NIR-IBBCEAS instrument. The separation between the transmitter and receiver units could be varied from 50 cm to 100 cm. 42

Figure 16: Inside view of Spectral Products tungsten-halogen light source. The circled portions are the lamp (bulb and focusing optics), cooling fan and electronics unit. 43

Figure 17: The temporal dependence of tungsten halogen lamp intensity at 1240.64 nm. Long term drift was calculated from the slope of the trend line as 0.72% per hour. Short-term fluctuation is approximately 7.2%. 44

Figure 18: A typical cavity signal obtained for a properly aligned NIR-IBBCEAS gas detector with a gain of 64. 47

Figure 19: The working prototype of NIR-IBBCEAS natural gas detector developed for the current study. The figure on the bottom left shows the inside view of transmitter unit and the bottom right figure depicts the receiver unit. The numbering is based on Figure 14. 48

Figure 20: A log-log plot of Allan variance as a function of averaging time for the mirror wavelength. At τ = 75 s, Allan variance showed a minimum, indicating maximum SNR... 51

Figure 21: The user interface of the NIR-IBBCEAS automation software. The plots displayed are for 995.1 ppm methane detection. Top figure corresponds to spectrum collection while the bottom figure displays the SVD fitting. 53

Figure 22: The experimentally determined reflectivity of the NIR-IBBCEAS detector instrument in the 1100-1250 nm range. The solid line represents a second-order polynomial fit to the calculated reflectivity values (dotted-line curve). The error bars indicate a one standard deviation of ± 0.00022 (fit uncertainty) from the fit. 56

Figure 23: Upper panel: Extinction coefficient of 995.1 ppm methane measured using the NIR-IBBCEAS instrument (dotted-line spectrum). The solid line denotes nonlinear least square generated according to equation 16. Lower panel: Absolute residuals of the fit. 63

Figure 24: Measured extinction coefficient of the mixture from the NIR-IBBCEAS instrument (dotted-line spectrum). The solid line denotes least square fit generated according to equation 16. 66

Figure 25: Overlapping absorption cross-section of propane and butane..... 67

Figure 26: The platform designed to place the tungsten-halogen lamp (bulb and focusing optics) dismantled from the original source box. It constitutes a top cover (A) and a base (B) where the former is attached over the latter by screwing them together. The lamp is fixed over the top cover while the base is attached to the breadboard. The dimensions are decided such that the center of bulb is at the required optical height. 107

List of Symbols, Abbreviations and Nomenclature

Symbol	Definition
PM	Particulate matter
VOC	Volatile organic compound
LNG	Liquified natural gas
GTL	Gas to liquid
GTW	Gas to wire
CNG	Compressed natural gas
GTS	Gas to solid
TDLAS	Tunable diode laser absorption spectroscopy
CRDS	Cavity ring-down spectroscopy
IBBCEAS	Incoherent broadband cavity enhanced absorption spectroscopy
CEAS	Cavity enhanced absorption spectroscopy
CAPS	Cavity attenuated phase shift spectroscopy
ICOS	Integrated cavity output spectroscopy
NICE-OHMS	Noise-immune cavity enhanced optical heterodyne spectroscopy
UV	Ultraviolet
IR	Infrared
MIR	Mid-infrared
NIR	Near-infrared
FIR	Far infrared
DBR	Distributed Bragg reflector
EOL	Environmental Optics Laboratory
MTU	Michigan Technological University
NITC	National Institute of Technology Calicut
FWHM	Full width at half maximum
ND	Neutral density
SNR	Signal to noise ratio
SVD	Singular-value decomposition
LEL	Lower explosive limits
L	Length of optical cavity/absorption length
α	Absorption coefficient
σ	Absorption cross-section/standard deviation
λ	Wavelength
I	Transmitted intensity through absorbing sample
I_0	Transmitted intensity through non-absorbing background
R	Reflectivity
n	Number density

Chapter 1: Introduction

1.1 Natural Gas and its importance

Industrial revolution during the 18th century marked the beginning of a new era in the energy sector through the gain in popularity of fossil fuels, mainly coal, to fulfill the ever-growing energy need of humankind. Since then, fossil fuels play a dominant role in the global energy market. They account for about 80% of primary energy consumption around the world (Goldemberg, 2006). Coal, oil and natural gas form the main fossil fuels which are non-renewable gifts from nature. Out of the total remaining reserves of fossil fuels, coal accounts for 65% of fossil fuel reserves in the world while oil and natural gas being the outstanding share. Moreover, coal reserves are widely distributed around the world while oil and gas are largely limited to the Middle East. It is also estimated that coal reserves would last for another 94 years while the depletion time for oil and natural gas reserves is approximately 23 years (Shafiee & Topal, 2009).

All the fossil fuels are composed of different hydrocarbon mixtures with varying ratios of hydrogen and carbon. This results in the emission of carbon dioxide and carbon monoxide on its combustion making it a major humanmade agent of global warming on a global scale (Olah, 2005). Focusing on its independent effects, combustion of coal for energy-related purposes results in the release of sulfur oxides, nitrogen oxides, particulate matter (PM) and other hazardous substances contributing to the increasing levels of urban air pollution, which is responsible for a large number of deaths yearly around the world. For instance, SO_2 and SO_4^{2-} released from burning coal were held responsible for London's "The Great Smog" in December 1952, killing more than 12,000 people and thousands of animals (Harrison, 2004; Molina &

Molina, 2004). Moreover, the domestic coal combustion, at times, involves the use of mineralized coal which would expose the local community to the toxic elements such as arsenic, fluorine, mercury, and antimony in the emissions. This can cause serious health issues such as arsenic poisoning, various forms of fluorosis and visual impairment (Finkelman, Belkin, & Zheng, 1999).

Use of petroleum products such as fuel oil, gasoline, and diesel oil add to the depletion of air and water quality around us. Such fuels are mainly used in the transportation sector and running power plants for electricity generation. Residual fuel oils used in power plants and ships contain high sulfur content (3-5%) by weight. Ships in particular, which do not have emission regulations, use high sulfur containing oils making it the most significant mobile SO_2 emitter (Sawyer et al., 2000). Even though the number of oil-powered power plants is fewer compared to the coal alternatives, the SO_2 emissions from oil consumptions are not negligible. For instance, in the year 1982, the sulfur emissions from oil usage in the United States were only less than 20% of that from coal (Husar, 1986). Oils are also used in jet aircraft which are high NO_x emitters (Baughcum, 1996; Gaffney & Marley, 2009). Apart from NO_x and SO_2, they also emit a huge amount of CO_2 during their complete combustion (99%) with incomplete combustion resulting in PM. Gasoline and diesel oils are no better when it comes to polluting the environment and causing health hazards. Lead emissions from gasoline, mainly in the form of inorganic lead halides, are extremely noxious for adults and children (Blokker, 1972; Finlayson-Pitts & Pitts Jr, 1986). Direct toxins such as carbon monoxide and indirect pollutants such as volatile organic compounds (VOC) and NO_x from gasoline and diesel fuels are also of great concern as they cause respiratory discomforts and result in ozone formation (Finlayson-Pitts & Pitts Jr, 1999). Diesel engines produce many times higher amount of NO_x per unit mass of fuel

than gasoline alternatives (Gaffney & Marley, 2009; Kirchstetter, Miguel, & Harley, 1998). In addition, gasoline combustion also releases toxic components such as benzene which is highly carcinogenic causing leukemia in humans (Aksoy, 1989; Gorse et al., 1991). Since the size of PM from diesel exhausts are very small (90% are less than 1 micrometer in diameter), it too can cause increased probability of lung cancer and respiratory morbidity (Lloyd & Cackette, 2001). However, natural gas is considered as the cleanest fossil fuel available today. Compared to coal and oil, natural gas combustion emits considerably lesser amounts of greenhouse gases and other toxic elements. The amount of carbon dioxide emitted per unit of energy produced from natural gas is approximately 50% of that from coal and one-fourth less than oil (Davies, 2001; Demirbas, 2006). Since it mainly contains lighter hydrocarbons, with lesser carbon content than coal and oil, it emits a very little amount of nitrous oxide and sulfur dioxide during its combustion. It releases virtually no ash or particulate matters helping to improve the air quality and reducing the extent of smog formation (Y. Wang, Xing, Xu, & Du, 2016). It is estimated that natural gas is about 65-70% less greenhouse intensive than coal (Chang et al., 2004; Roarty & Roarty, 2008). There has been increased advocacy of natural gas-powered vehicles considering its energy and environmental benefits. These include reduced NO_x, $PM_{10,}$ VOC and CO emissions. There are different natural gas based fuels used in transportation today which can minimize the fossil energy use per mile (M. Q. Wang & Huang, 2000). Over the last two decades, advanced research is being carried out in the field of developing enhanced engine functionalities and engine designs towards achieving zero emissions in natural gas-powered vehicles. This was made possible through the development of lightweight high-pressure storage cylinders (Kato et al., 1999). Apart from its environmental advantages, natural gas is a lot safer compared to petroleum in many aspects (Kowalewicz, 1984). Natural gas is about 40% lighter

than air and hence disperses upward swiftly, in case of spillage, unlike diesel and gasoline puddling on the ground creating an extreme fire danger. The ignition temperature of natural gas is quite high with narrow combustible range making it less risky than the petroleum alternatives (Semin, 2008).

Due to these benefits, the demand for natural gas has observed a surge for the past several years and is predicted to increase annually by 2.8% from 2001 to 2025 (Demirbas, 2006).

1.1.1 Distribution of Natural Gas

The increasing demand for natural gas must be satisfied through an efficient transport system for moving the gas from the extraction points, which are often remote areas, to the commercial markets and the end consumers. Different methods are being utilized today for transporting gas. These include pipelines, liquified natural gas (LNG), gas to liquids (GTL), gas to wire (GTW), compressed natural gas (CNG) and gas to solids (GTS-hydrates). Pipelines have been employed for this purpose for a long time, which are extremely useful for short distance transport. As the distance increases, they face technological and political restrictions along with economic drawbacks. Long distance pipelines can become expensive and lead to high capital investment with less returns. Cross country pipelines often involve various political and regulatory environments hindering its development. Pipelines are also considered to be inflexible to an extent, and its closure forces the shutdown of the production and collection points due to storage issues (Mokhatab & Poe, 2012). Hence, over the past few decades, new techniques have been attempted to transfer gas efficiently. One such method is to liquefy natural gas at -162^{o}C and transport it to distant destinations. Even though this technique is expensive, the incremental cost of transport per mile is lesser. In GTL, the gas is converted to a liquid through a stage of syngas

conversion, before transferring it. However, this comes with substantial emission from GTL plants and their units. GTW is used in cases where the end application of natural gas is to generate electricity. In this method, electricity produced using the gas at its production facility is transported via high voltage transmission lines. This can, however, cause serious power loss and expensive transmission line installments. Another idea is to compress the gas in containers at high pressure (1800 to 3600 psi) and move it to the destination (CNG). However, this can get complicated at times, as one must know the thermodynamics of gas expansion and compression and to utilize appropriate gas networks, compressors, and heat exchangers, adding additional costs. Research is also performed on the viability of transferring gas by converting it into solids or slurries of gas hydrates (GTS) (Thomas & Dawe, 2003). All these alternatives are in their developing stage while pipelines continue to dominate the gas transportation market.

1.1.2 Challenges of Natural Gas Distribution

Transporting natural gas is accompanied by the risk of leakage. Hundreds of thousands of valves and flanges, along with thousands of kilometers long pipeline networks are all prone to leakage. Such gas escapes are believed to be the largest contributor to the anthropogenic methane emissions in the United States (almost 40%) (Howarth et al., 2012). Studies on gas leakages during distribution are also reported from other parts of the world including Russia and UK (Dedikov et al., 1999; Lechtenböhmer et al., 2007; Mitchell, Sweet, & Jackson, 1990). Apart from this, the natural gas leak can also occur during the production and consumption stages. A study by Allan et al., reported that the production stage methane emissions from around 150 sites in the US were about 0.42% per unit gross gas production (Allen et al., 2013). However, airborne

measurements in the gas wells in the Unitah county reported an hourly emission rate of about 6.2% to 11.7% of the average hourly production (Karion et al., 2013).

Apart from the economic losses, such leaks and emissions can have an adverse impact on the environment and health of living beings. Even though natural gas is considered to be cleaner than other fossil fuels due to its low carbon dioxide emissions, natural gas leaks emit methane into the atmosphere. Methane is one of the most important greenhouse gases contributing to the global rise in temperature. Among the non-CO_2 greenhouse gases, methane results in the largest net climate forcing. In fact, studies claim that natural gas spillage of 4% or more (including extraction, distribution and consumption stages) would nullify the benefits of low carbon dioxide emissions by switching from coal to natural gas (Hansen, Sato, Ruedy, Lacis, & Oinas, 2000; Rodhe, 1990). Natural gas extraction through drilling and hydraulic-fracturing have also contributed to ground and drinking water contaminations with observed values of methane and ethane concentrations well above the hazard levels (Jackson et al., 2013; Osborn, Vengosh, Warner, & Jackson, 2011). Natural gas leakage can also affect the biological and chemical processes in the soil along with vegetation (Hoeks, 1972). Hence, it is extremely important to monitor natural gas leaks and implement preventive measures to curb them.

Analogous to the risk of leakage, another important feature associated with the supplied natural gas is its composition and end quality. Even though methane forms the major component of natural gas with some amount of other light hydrocarbons and nitrogen, the exact composition of a natural gas mixture depends on the source. This results in the substantially varying composition of the final usable gas supplied around the world, even within the United States (King, 1992). The percentage of methane by volume ranges from 56% to 98% while that of ethane can vary between 0.5% to 13.3%. Amount of propane can take values between 0% to 23.7% by volume

with lower amounts of heavier hydrocarbons like iso-butane, n-butane (0 to 1%) and pentane (trace) (Liss, Thrasher, Steinmetz, Chowdiah, & Attari, 1992). Significant fractions of nitrogen and carbon dioxide are also present in a typical natural gas mixture with trace amounts of sulfur compounds meant to serve as odorants (Amirante et al., 2017). Studies have shown that the composition of end-used natural gas affects the engine operational properties and fuel metering. In a lean-burn engine, it could result in misfire due to its effect on lean flammability limit of the mixture, while in the direct-injection diesel engines, it affects the autoignition delay (King, 1992; Naber, Siebers, Di Julio, & Westbrook, 1994). The varying composition can also affect the level of pollutant emissions in the natural gas-powered vehicles due to the variation in Wobbe index and air-fuel ratio (Ly, 2002). Hence, it is equally vital to determine the quality of end-used natural gas.

1.2 Contemporary Natural Gas Leak Detection Techniques

Across the world, different methods are employed for identifying natural gas emissions from point and non-point sources (Carlson, 1993). One of the primitive efforts was to add an odorant, a mercaptan also known as thiol (pungent or rotten egg smelling substance), to the otherwise colorless and odorless natural gas (Speight, 2007). This assisted experienced personnel or trained dogs to locate leaks by its odor, sound or just visual inspection. Currently, owing to the advancement of scientific research, numerous techniques are available to serve this purpose (Scott & Barrufet, 2003; Sivathanu, 2003; Zhang, 1997). These techniques can be broadly divided into non-optical and optical methods (Figure 1). Non-optical methods can be further classified into hardware and software-based techniques while optical techniques can be grouped as active or passive methods.

1.2.1 Non-Optical Techniques

Primary non-optical techniques are based on the principles of acoustic monitoring, gas sampling, soil monitoring, flow monitoring and dynamic model-based system. As the name suggests, acoustic monitoring is based on the acoustic emissions at the leak points (Hough, 1988; Klein, 1993). Acoustic sensors detect the change in background noise pattern due to the leak emissions and thereby locating its position without interfering with the pipeline operations. However, a very large number of sensors are required to do this for the whole length of the pipeline. Since a substantial acoustic emission signal intensity is required to differentiate it from the background noise, small leaks cannot be detected efficiently. Gas sampling methods employ a methane detector or a flame ionization detector to detect gas leaks. Such devices can be hand-held or mounted on vehicles and carried along the pipeline (Sperl, 1991). Even though this technique is highly sensitive for detecting minute leaks and has a narrow chance of generating a false alarm,

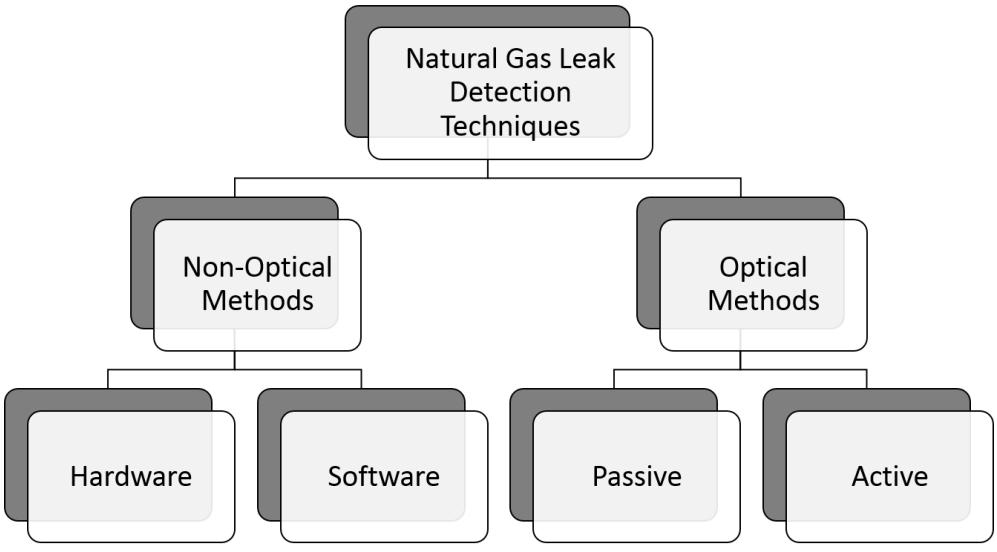

Figure 1: Review of natural gas leak detection methods.

it is usually combined with systems such as gas chromatography and hence, the total time to obtain a quantitative result can be long (Sivathanu, 2003). The results are also limited to the sampling area from which the gas is drawn and hence, the technique is usually quite expensive. Soil monitoring is similar to the idea of adding thiols into the gas, as discussed earlier. In this method, a tracer chemical is added to the pipeline along with the natural gas (Thompson, 1991). An appropriate detection system for this chemical is installed along the surface of the pipeline to observe any oozing of the chemical from the leaks. This is a highly sensitive and reliable technique. However, the cost of monitoring leaks using soil monitoring is quite high. Flow monitoring technique could be either based on pressure or mass flow at different locations within the pipeline (Bose & Olson, 1993; Turner, 1991). If there is a considerable difference in the rate of change of pressure or mass flow at two locations in a pipe, it could be due to a potential leak. This is a low-cost technique to detect leaks but with huge false alarm rates. It is also not possible to determine the exact location of the leak using this method. In software-based dynamic modeling, the gas flow through the pipeline is modeled mathematically using various flow parameters along the pipeline. The natural gas leaks are then detected based on the discrepancies between calculated and measured values at different locations (Griebenow & Mears, 1989; Liou & Tian, 1995). This technique can be used to monitor leak continuously without affecting the pipeline functions. However, these are expensive for monitoring large networks of pipes with a higher rate of false alarm.

1.2.2 Optical Techniques

Optical techniques, typically, utilizes the spectroscopic properties of the gas (absorption or scattering of light by the gas molecules). Division of optical techniques into passive and active

depends on the need for a source of light. In passive optical monitoring technique, an external light source is not required as the radiation emitted by the natural gas or the background serves as one. This means that weak radiations are to be detected which requires much more expensive detectors and imagers. Two prominent passive techniques employed for natural gas detection are thermal imaging and multi-wavelength imaging. Thermal imaging is based on the difference in temperature between the gas and surroundings (Kulp, Powers, & Kennedy, 1997; Weil, 1993). This is a portable technique with a wide spatial coverage. However, the costly thermal imagers and the requirement of a temperature difference between the gas and surroundings reduce its applicability. Multi-wavelength absorption imaging maps the gas concentration using the background absorption at multiple wavelengths (Althouse & Chang, 1995; Bennett, Carter, & Fields, 1995). This does not require a temperature difference and is less prone to a false alarm. However, as mentioned before, the detection units for such systems are very expensive.

Unlike the passive counterparts, active optical monitoring techniques employ a laser source or a broadband light source to irradiate the region over the pipelines and look for absorption or scattering caused by the natural gas molecules at specific wavelengths using detectors and sensors. Presence of such spectroscopic signatures presumes the presence of a leak. Typical techniques employed in this category include Lidar systems, Tunable Diode Laser Absorption Spectroscopy (TDLAS), backscatter imaging, Millimeter Wave Radar systems and Cavity Ring-Down Spectroscopy (CRDS). Lidar system uses a pulsed laser as the illuminating source. The leak is identified based on the absorption of its energy along the sampling length (Ikuta et al., 1999; Minato, Joarder, Ozawa, Kadoya, & Sugimoto, 1999). A pulsed laser is quite expensive with higher chances of a false alarm due to its single wavelength monitoring. The principle of TDLAS is similar to that of Lidar systems. The main difference between the two lies in the

source where TDLAS employs a tunable diode laser instead of the pulsed laser (Iseki, Tai, & Kimura, 2000). TDLAS has two advantages over Lidar systems. Since diode laser is cheaper compared to the pulsed laser, TDLAS is economical out of the two. Moreover, the tunability feature allows detection to be carried out in more than one wavelength. This reduces the rate of false alarm quite a bit. However, compared to broadband sources, TDLAS is still expensive and prone to false alarms as the tunability is based on a comparatively smaller range of wavelength. In backscatter imaging, as the name suggests, the backscattered light by the natural gas molecules is imaged to pinpoint the leak (Kulp, Kennedy, DeLong, Garvis, & Stahovec, 1993). A carbon dioxide laser is used for this method along with infrared imagers and detectors. Millimeter Wave Radar systems, on the other hand, uses a radar signature generated due to the density difference of methane and air as an indicator for detecting potential leaks (Gopalsami & Raptis, 2001). Even though both techniques are portable and have remote monitoring capabilities, they are quite expensive for its deployment and maintenance. The principle of CRDS based leak detection is based on the decay time of laser light inside an optical cavity. This technique is highly sensitive due to long effective path length created by the high reflective mirrors (Jackson et al., 2014). However, they are mainly based on a single wavelength approach making it prone to a false alarm.

1.3 Motivation for This Thesis

Apart from having remote monitoring features, an ideal natural gas leak detection technique should also be low-cost, efficient, sensitive and reliable. However, from the review of the existing methods, it is evident that none of the current technology possesses all these attributes. The main competition is between the rate of false alarms and cost-effectiveness. Hence, the aim

of this thesis is to develop a working prototype of a natural gas leak detector with all the aforementioned qualities along with the additional capability of estimating the natural gas composition. This work exploits the principle of Incoherent Broadband Cavity Enhanced Absorption Spectroscopy (IBBCEAS) in the near-infrared (NIR) region of the electromagnetic spectrum to detect and quantify the major hydrocarbons of a natural gas mixture, viz., methane, butane, ethane, and propane. Chapter two describes the principle of IBBCEAS in detail along with its benefits over other absorption spectroscopic techniques like CRDS. The chapter also details the importance and previous applications of the NIR region in the hydrocarbon detection. The NIR-IBBCEAS approach was also employed to obtain the absorption spectra and reference cross-sections of the individual hydrocarbons for their quantitative evaluation. Chapter three presents these measurements along with some insights on the calibration schemes performed. In chapter four, the hardware and software development of the NIR-IBBCEAS natural gas leak detector is explained while chapter five comprises of the information on data analysis and instrument characterization. A section on summary and scope of improvements concludes the thesis.

Chapter 2: Incoherent Broadband Cavity Enhanced Absorption Spectroscopy

Optical gas detection techniques mainly employ the scattering or absorption signatures of the gas in different regions of the electromagnetic spectrum. The methods based on scattering detect a portion of incident light scattered by the gas molecules while those based on absorption measure the amount of light absorbed by them. Absorption spectroscopy is considered as a simple, non-invasive procedure utilized widely for *in situ* detection of trace gas species in the atmosphere (J. Chen, 2011).

2.1 Absorption Spectroscopy

Absorption spectroscopy is a spectroscopic technique used to measure the concentration of absorbing gas (or liquid) by looking at its absorption of electromagnetic radiation in a wavelength (or frequency) region (Nilapwar, Nardelli, Westerhoff, & Verma, 2011). The basis for most of the conventional optical absorption methods is the Lambert-Beer law. The law relates the amount of light absorbed to the concentration of the species within the given path length. For gaseous (or liquid) absorbers, the law could be formulated as (Platt & Stutz, 2008),

$$I(\lambda) = I_o(\lambda) * e^{(-\sigma(\lambda)*c*L)}, \quad (1)$$

Here, $I_0(\lambda)$ denotes the initial intensity of radiation without any absorbing species, while $I(\lambda)$ represents the intensity of radiation after passing through the region of length L containing a uniform concentration of absorbing species, c. $\sigma(\lambda)$ is the wavelength dependent absorption cross-section, which is a characteristic property of the species. The product of absorption cross-

section and concentration is known as absorption coefficient. Equation (1) implies that the concentration of absorbing species can be deduced by measuring the ratio $I_0(\lambda)/ I(\lambda)$ along with knowledge of absorption cross-sections and path length (Figure 2).

It also denotes the relation between measurement sensitivity and optical path length. Longer

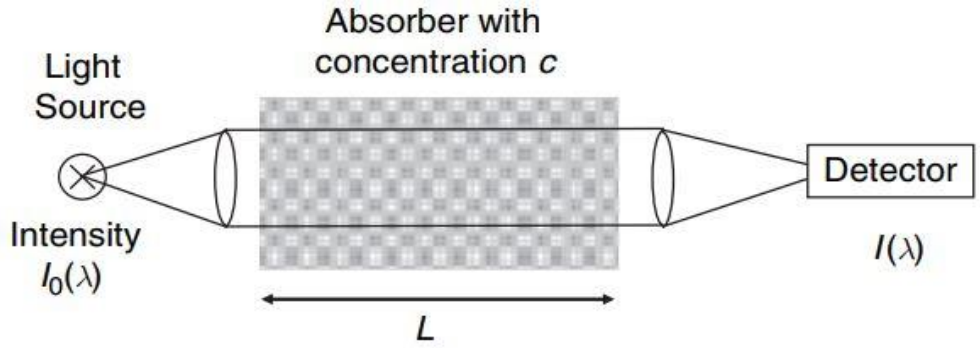

Figure 2: Application of absorption spectroscopy for gas detection (Platt & Stutz, 2008).

effective pathlength results in a higher sensitivity (or lower minimum detection limits). Long optical pathlength could be achieved either by physically placing the source and detector far apart or by reflecting the light multiple times through the absorbing sample in small dimensions (D. Venables, 2016). Over the course of advancement in absorption spectroscopy, different techniques have been introduced to achieve longer path lengths. Traditional schemes utilize multi-reflection cells described by White (White, 1976) or Herriot and Schulte (Herriott & Schulte, 1965) to obtain improved effective interaction lengths and hence, improved detection limits (Nägele & Sigrist, 2000; Peter Werle et al., 2002). However, such arrangements get complicated when hundreds of optical passes are required. They also demand highly stable mechanics for its optical alignment. A more recent approach is to make use of high finesse optical cavity for high sensitive trace gas measurements. Such high finesse optical cavities can improve the effective optical path lengths to thousands of passes (Daniele Romanini, Ventrillard, Méjean, Morville, & Kerstel, 2014). Two major variants of absorption measurements using the

optical cavities are the ones utilizing temporal dependence of light inside the cavity and the ones based on transmitted intensity. Cavity Ring-Down Spectroscopy (CRDS) dominates the former type, which measures the rate of decay of photons inside the cavity. Introduction of this technique marked the beginning of exploiting optical cavities for extremely sensitive measurements (O'Keefe & Deacon, 1988). The techniques based on transmitted intensity are broadly grouped under Cavity Enhanced Absorption Spectroscopy (CEAS), which measures the intensity of light transmitted through the optical cavity.

Similar to optical pathlength, another important factor affecting the gas detection is the choice of light source. Pulsed laser, continuous-wave laser, tunable diode lasers and spectrally broadband light sources are some of the widely used alternatives for sensitive gas detection (Berden & Engeln, 2009; Engeln & Meijer, 1996; O'Keefe & Deacon, 1988; D Romanini, Kachanov, Sadeghi, & Stoeckel, 1997; Schiff, Mackay, & Bechara, 1994; PO Werle, Mücke, & Slemr, 1993). While the laser-based techniques have a higher signal to noise ratio and target gas specificity, broadband sources are best suited for simultaneous multiple species detections which require a wide spectral coverage than a high spectral resolution. Apart from avoiding the procedures of mode matching, broadband sources can also reduce the complexity and instrument cost compared to the laser variants. A broadband adaptation of CEAS is the Incoherent Broadband Cavity Enhanced Absorption Spectroscopy (IBBCEAS).

2.2 Principle of IBBCEAS

First demonstrated by Fiedler et al. (Fiedler, Hese, & Ruth, 2003), IBBCEAS is considered as the hybrid between conventional absorption techniques and CEAS. The method combines the multiplexing properties of the broadband methods with a high detection sensitivity of CEAS maintaining the experimental simplicity. Figure 3 depicts a typical IBBCEAS system employed for trace gas detection.

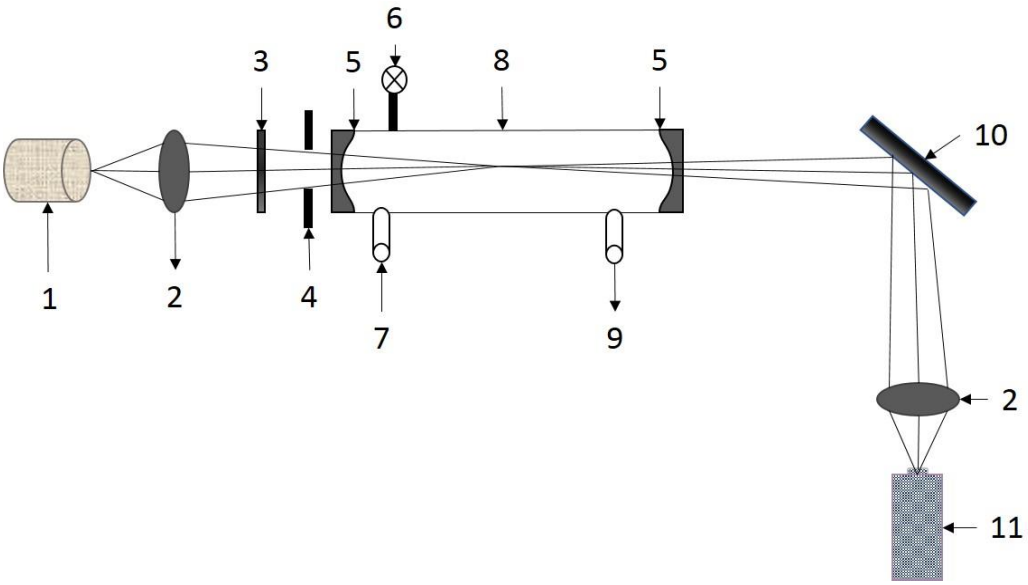

Figure 3: Schematic of an IBBCEAS system. 1, Incoherent broadband source; 2, focusing lens; 3, filter; 4, iris; 5, high reflective cavity mirrors; 6, pressure gauge; 7, gas inlet; 8, cavity cell; 9, gas outlet; 10, aluminum coated mirror; 11, spectrometer.

In this method, light from an incoherent broadband source like LED, arc lamps or supercontinuum sources, is detected after being transmitted through a stable optical cavity composed of two highly reflective mirrors (Fiedler et al., 2003; D. Venables, 2016). High reflective mirrors result in the back and forth bouncing of photons between them, before gradually leaking out of the resonator. This results in a long effective path length and increased interaction of gas molecules with the photons inside the optical cavity. The transmitted intensity

is then detected using a spectrometer or a combination of the grating spectrograph and sensitive CCD detector. A set of filters (low pass, high or band pass filters) are also employed in the set up to eliminate stray lights to avoid spectrometer saturation due to the relatively weaker nature of cavity transmission signal. The input light is also collimated upfront to avoid undesirable intensity loss and scattering effects. Measurement of absorption coefficient using IBBCEAS is according to the superposition principle for ring down cavities (Lehmann & Romanini, 1996). It exploits the benefit of spectrally broad light to overlap a large number of resonant cavity modes and generate a continuous transmission output thereby eliminating the need for any mode-matching scheme. It also assumes negligible nonlinear influences and a large detector bandwidth (> free spectral range of the cavity which is defined as the separation between two adjacent resonance peaks in the frequency domain) for it to be insensitive to intensity variations caused by the eigenmode structure of the resonator (Fiedler et al., 2003). Sensitive absorption measurements using IBBCEAS can be performed in a closed cell or open path configuration (Gherman, Venables, Vaughan, Orphal, & Ruth, 2008; Varma et al., 2009). Unlike open path setup, a closed path configuration provides a long-time stable and rigid cavity structure but may be prone to inlet and wall sample losses.

For any qualitative or quantitative IBBCEAS measurements, the transmitted spectrum through an empty stable optical cavity (without the absorbing species), $I_0(\lambda)$ is recorded initially. This is followed by the measurement in the presence of absorbing species, $I(\lambda)$. If L [cm] denotes the length of the optical resonator, then the absorption coefficient, $\alpha(\lambda)$ [cm^{-1}] of the gas species inside the cavity is determined using (Fiedler et al., 2003),

$$\alpha(\lambda) = \frac{1}{L}\left(\frac{I_0(\lambda)}{I(\lambda)} - 1\right)\left(1 - R(\lambda)\right), \quad (2)$$

where *R(λ)* is the mirror reflectivity. If the absorbing mixture comprises of multiple absorbing species, the measured absorption coefficient can be broken down into contributions from individual species due to their structured absorption (Equation 3) (Adams, 2016; Varma et al., 2009).

$$\alpha(\lambda) = \sum_i \sigma_i(\lambda) \int_0^L n_i(x)dx, \quad (3)$$

where n_i is the number density of i^{th} species [molecule cm^{-3}], and $\sigma_i(\lambda)$ is its wavelength-dependent absorption cross section [cm^2 $molecule^{-1}$].

One of the drawbacks of this technique is the requirement of determining cavity mirror reflectivity as a function of wavelength for any quantitative estimations. To retrieve absolute concentrations of the absorbing species, IBBCEAS requires an independent reflectivity calibration measurement. This can be done in different ways. One method is to introduce a known concentration of absorbing gas inside the cavity which has an absorption feature in the spectral range of interest. With the knowledge of its absorption cross-section from literature and spectroscopic databases like HITRAN, the reflectivity of the mirrors can be determined with the help of the following equation (D. S. Venables, Gherman, Orphal, Wenger, & Ruth, 2006).

$$R(\lambda) = 1 - \sigma(\lambda) nL \left(\frac{I_0(\lambda)}{I(\lambda)} - 1 \right)^{-1}, \quad (4)$$

Here, $I(\lambda)$ and $I_0(\lambda)$ are the intensities transmitted through the resonator with and without the absorbing gas and $\sigma(\lambda)$ is absorption cross-section [cm^2 $molecule^{-1}$] from literature while n denotes its number concentration [molecule cm^{-3}]. The next idea is to add gases with different Rayleigh scattering cross-sections. In this technique, $R(\lambda)$ is deduced based on the change in transmitted intensity due to Rayleigh scattering, when the cavity is filled with two different scattering gases (Axson et al., 2011; Washenfelder, Langford, Fuchs, & Brown, 2008).

$$R(\lambda) = 1 - \left(\frac{\frac{I_{gas1}}{I_{gas2}} \alpha_{Ray}^{gas1} - \alpha_{Ray}^{gas2}}{1 - \frac{I_{gas1}}{I_{gas2}}} \right) L, \quad (5)$$

Here, α_{Ray} denotes the Rayleigh scattering coefficient for the gas. Another useful method for reflectivity calibration, particularly for open path configurations, is to use an antireflection-coated optical substrate whose loss as a function of wavelength ($Loss(\lambda)$) is known. In this case, the mirror reflectivity can be calibrated as follows (Varma et al., 2009):

$$R(\lambda) = 1 - \left(\frac{I(\lambda)}{I_0(\lambda) - I(\lambda)} Loss(\lambda) \right), \quad (6)$$

IBBCEAS is certainly just one of the many spectroscopic techniques available today, for sensitive gas detection. However, IBBCEAS achieves absorption enhancements comparable to other methods maintaining experimental simplicity and robustness of the traditional non-invasive optical absorption spectroscopy techniques (J. Chen, 2011). Some of the spectroscopic procedures which enhances the minimum detection limits and photon-molecule interactions include CRDS (O'Keefe & Deacon, 1988), broadband CRDS (Ball & Jones, 2003), Cavity Attenuated Phase Shift Spectroscopy (CAPS) (Kebabian & Freedman, 2007), Integrated Cavity Output Spectroscopy (ICOS) (O'Keefe, Scherer, & Paul, 1999), Noise-Immune Cavity Enhanced Optical Heterodyne Spectroscopy (NICE-OHMS) (Foltynowicz, Schmidt, Ma, & Axner, 2008) and Cavity enhanced dual comb spectroscopy (Bernhardt et al., 2010). Most of them achieve increased sensitivity at the expense of overall cost and experiment difficulty. Except for CAPS, all the other above-mentioned techniques usually make use of a laser system to detect gas species. The normal narrowband continuous-wave laser limits the applicability of the technique to single species detection. To attain a multi-component detection feature, they must be equipped with additional components like optical parametric oscillator system to facilitate wavelength scanning over a small range. Some of them also employ a mode-locked laser and mode matching schemes to enhance the coupling efficiency. All these efforts add to the complexity and cost of instrumentation (Aalto, Genty, Laurila, & Toivonen, 2015; Hodgkinson & Tatam, 2012). CAPS, on the other hand, uses a broadband source like IBBCEAS but requires a modulation routine and lock-in amplifiers, making it no better. Even though unlike IBBCEAS, techniques like CRDS do not require a calibration standard for absolute concentration retrieval, it depends on the high-speed electronics triggering and detection. Like some of the other CEAS techniques, CRDS is also susceptible to vibrations and precise alignment requirements. Even though techniques like

off-axis alignment have found a solution for vibrational effects (Paul, Lapson, & Anderson, 2001), the resonator's mode structure tend to become unstable in such efforts (Karpf & Rao, 2015).

IBBCEAS on the other hand is less sensitive to alignment and require only basic electronics for its operation. The spectrally broad light implies effective coupling with numerous cavity modes without any additional mode-matching techniques along with the feasibility of multi-species detection (Tao Wu, Coeur-Tourneur, et al., 2014). Their compact and uncomplicated design along with its instrument stability, if carefully designed, makes it best suited for *in situ* and real-time field measurements, owing to its portability (Tao Wu, Zha, et al., 2014). Due to the broadband monitoring property, gas detectors based on IBBCEAS will also be less prone to false alarms. Additionally, the availability of cheap incoherent broadband sources like LEDs makes it a low-cost technology. All these features along with similar levels of sensitivities achieved through IBBCEAS compared to other spectroscopy techniques (Y. Chen et al., 2016) makes it a potential technology for developing a low cost, sensitive and reliable remote monitoring gas detector.

2.3 NIR-IBBCEAS for Natural Gas Detection - Present work

Generally, absorption spectroscopy could be applied for gas sensing and aerosol measurements in any portion of the electromagnetic spectrum between ultraviolet (UV) and far infrared (FIR). IBBCEAS, in particular, has found its extensive application in the UV (Gherman et al., 2008; Min et al., 2016; Washenfelder, Flores, Brock, Brown, & Rudich, 2013) and visible (Triki, Cermak, Méjean, & Romanini, 2008; Washenfelder et al., 2008; Tao Wu, Zhao, Chen, Zhang, &

Gao, 2009; Zhao et al., 2013) regions. The infrared (IR) section, comprised of NIR (0.8 to 2.5 μm,), Mid IR (MIR-2.5 to 25 μm) and FIR (25 to 1000 μm), is a reliable region for identifying organic compound and functional groups. The lower energy FIR region is usually used for rotational spectroscopy while the former two are used for studying the rotational-vibrational properties of samples. NIR is mainly composed of overtones and combinational bands while MIR contains the fundamental vibration bands of molecules (Siesler, Ozaki, Kawata, & Heise, 2008). Today, even though MIR region offers more specificity and selectivity than NIR region, the MIR instrumentation can be quite expensive compared to NIR. Water vapor interference also poses a problem in MIR spectroscopy while it is negligible in the NIR range (Peter Werle et al., 2002). Moreover, for simultaneous detection of multiple gas species, the weak overtone bands in NIR can be of greater use than the strong fundamental absorption bands in the MIR region. The technological developments in the field of telecommunication have resulted in inexpensive light sources and spectrometers in the NIR regime, facilitating the development of NIR spectroscopy as a powerful optical technique for gas sensing applications (McClure, 1994; Pasquini, 2003). All these factors contributed to the selection of NIR region for hydrocarbon absorption study in this work.

In the recent times, IBBCEAS and variations of IBBCEAS technique have been successfully extended to the NIR region for detection of species like CO_2, Carbonyl sulfide (Orphal & Ruth, 2008), ether-1,4-Dioxane (Chandran & Varma, 2016) and 1,3-butadiene (Denzer et al., 2009). In 2014, Rohwedder et al., also showed that all the major hydrocarbons of a natural gas sample have absorption signatures in the NIR region between 900 and 1650 nm (Rohwedder et al., 2014). Hence, this thesis presents the first application of IBBCEAS technology in the NIR regime for the detection of methane, ethane, propane, and butane, which forms the dominant

components of the natural gas mixture. The instrument exploits their absorption signatures in the wavelength range of 1100 to 1250 nm.

2.3.1 Component Details

The light source is an important part of IBBCEAS instrument which decides the performance of the whole system. One of the desirable characteristics of a light source is high radiance in the spectral region of interest. Tungsten-halogen lamps are usually the preferred source for NIR instruments due to its high spectral output between 360-3000 nm region and long lifetime (McClure, 1994). The light source used in this instrument was a 75 W, 1400 lumens tungsten-halogen lamp from Spectral Products (ASBN-W-075B). The company promises nominal lifetime of 2000 hours when driven by a 12-volt DC voltage regulated power supply supplied along with the lamp by Spectral Products. The setup houses a NIRez spectrometer with InGaAs detector from ISUZU optics, Taiwan, to detect the transmitted light. It has a detection wavelength range of 900 to 1700 nm. The spectrometer comes with measurement software, ISUZU_NIRez_eng, and a USB port to serve as a communication interface and power supply. The optical cavity was made out of two 1” high reflective distributed Bragg reflector (DBR) mirrors from Layertec GmBH, Germany. The mirrors exhibit a reflectivity of more than 99.8% in the wavelength range of 1100 and 1250 nm with a maximum reflectivity close to 99.9%. Optical cavities made of such highly reflective mirrors serve as an efficient band rejection filter (J. Chen, 2011). However, light outside the wavelength range of high mirror reflectivity can pass through the cavity without any rejection. Hence, a set of low pass and high pass filter from Edmund Optics, USA, was used to avoid the wavelengths outside the mirror range, thereby avoiding spectrometer saturation and other stray light problems. The precision short pass filter has a cut-off wavelength of 1250 nm

while the long pass filter has a cut-on wavelength of 1100 nm. All other focusing optics (combinations of lens and mirrors) were bought from Thorlabs, Inc., USA. The automation and remote controlling of the data collection and real-time analysis was done using LabVIEW software.

Chapter 3: Initial Testing and Calibration

3.1 Qualitative Testing

Even though the idea of applying NIR-IBBCEAS in the wavelength range from 1100 to 1250 nm appeared to be a promising technique to detect the major hydrocarbons, it is essential to test the method's feasibility in the lab before developing the prototype of the leak detector. This was carried out by setting up an BBCEAS (broadband cavity enhanced absorption spectroscopy) system in the Environmental Optics Laboratory (EOL) at Michigan Technological University (MTU), Houghton, USA. The experiments were supervised by Dr. Ravi Varma, Associate Professor, National Institute of Technology Calicut, India and Dr. Claudio Mazzoleni, Associate Professor, Physics, MTU, who provided valuable inputs and suggestions in that preliminary testing.

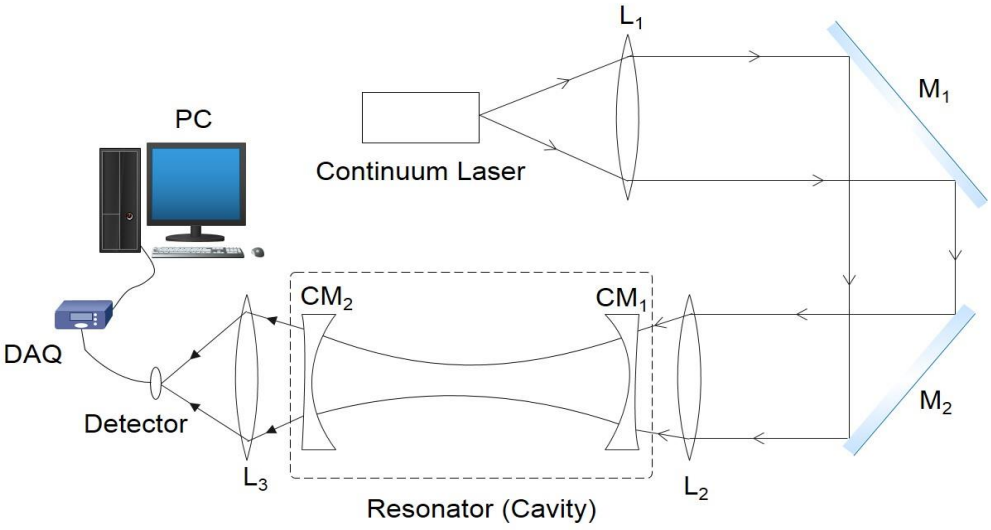

Figure 4: BBCEAS system set up in EOL, MTU. Here, L denotes 1" lens, CM represents cavity mirror and M denotes aluminum-coated mirror.

The BBCEAS arrangement installed in EOL is illustrated in Figure 4. It employed a supercontinuum laser, SC400 from Fianium Ltd. (currently NKT Photonics, Denmark) as the radiation source along with an Acousto-Optic Tunable Filter (AOTF) system for wavelength scanning. The choice of supercontinuum laser over the tungsten halogen lamp for this study was mainly due to two reasons. Supercontinuum laser provided a more stable light output when compared to the tungsten halogen source. Since a less noisy spectra was necessary to validate the absorption peaks of gases with the results from the study by Rohwedder et al., (Rohwedder et al., 2014), supercontinuum laser seemed to be a better option. Secondly, the laser system provided user-control over the output power. This made it possible to obtain an idea on the required power of the light source to be used in the IBBCEAS detector system. The laser operating power was set to 0.2 W (10% of its maximum value). The light from the supercontinuum laser was guided and coupled into an optical resonator using a system of 1" lenses and aluminum-coated mirrors. The 97.5 cm long optical cavity was formed using the DBR mirrors purchased for the instrument from Layertec GmBH, Germany. The cavity volume was closed using a 90 cm long steel pipe of

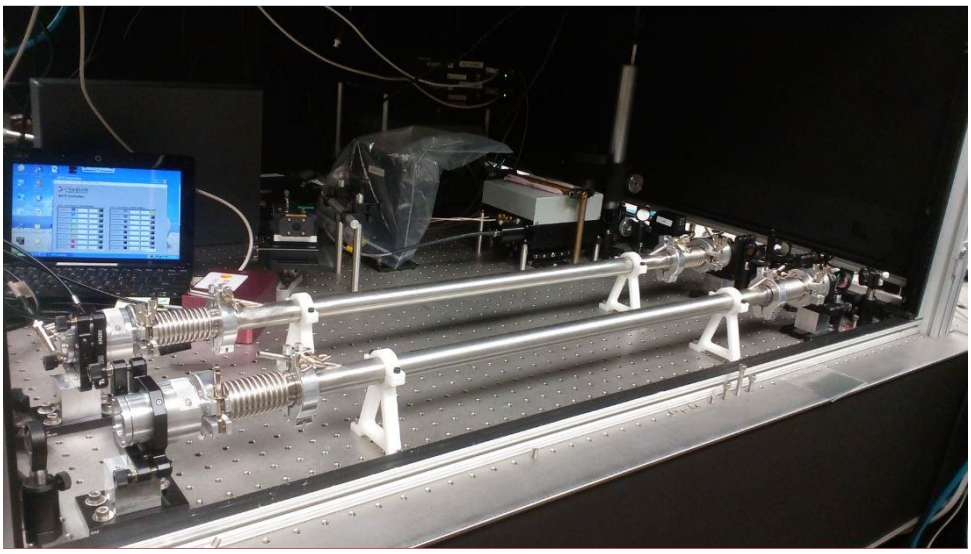

Figure 5: IBBCEAS set-up installed at EOL for qualitative testing of methane and butane detection.

1” diameter with a compatible vacuum bellow inserted between the pipe and mirror holder on both ends. The pipe also had an inlet and outlet to facilitate gas flow. The transmitted light from cavity was further detected using a photodiode (PD) after focusing it using a 1” lens. The information from photodiode was then interfaced into a computer using a National Instruments Data Acquisition card (NI DAQ). A LabVIEW program was also developed for data logging and analysis. The entire IBBCEAS system was installed on the top of an optical breadboard table (Figure 5).

According to Rohwedder et al., in the wavelength range of 1100-1250 nm, methane exhibits the lowest absorbance while butane shows the highest for same concentrations of both the gases

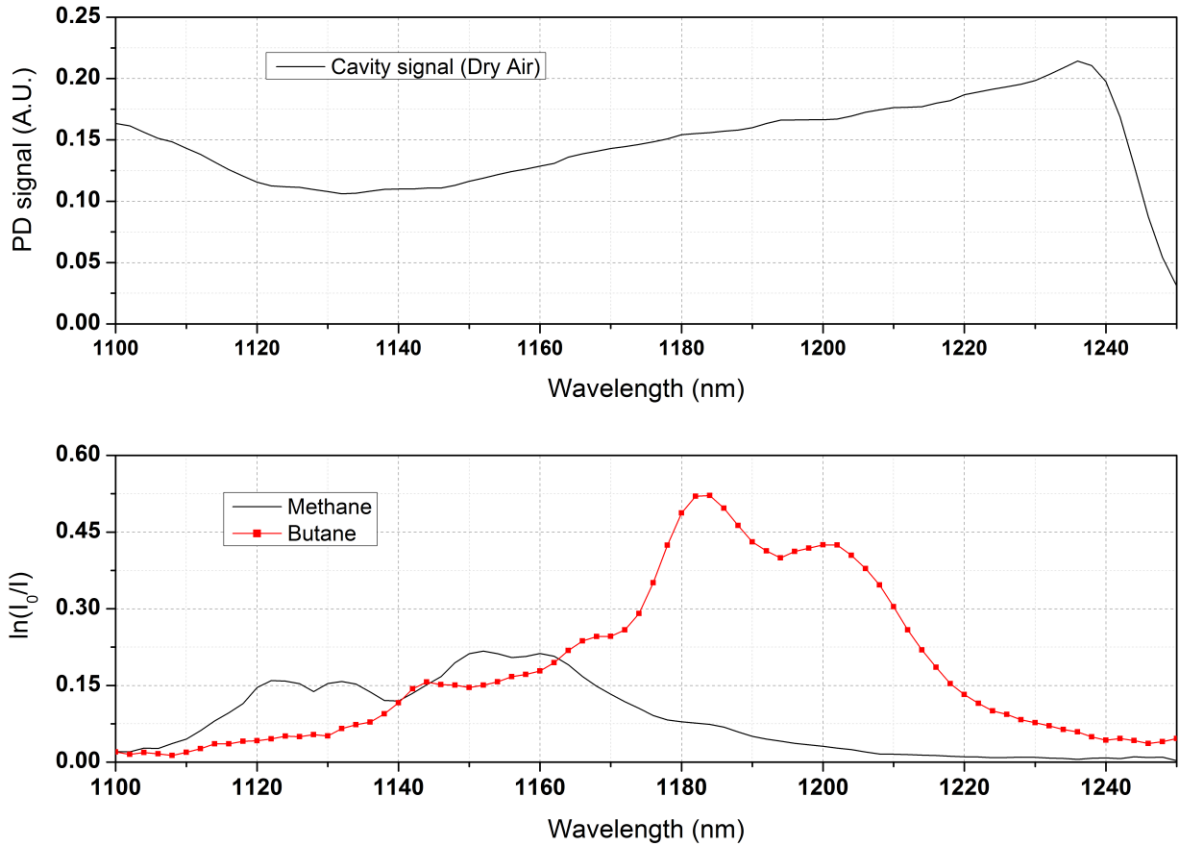

Figure 6: Top graph: PD signal generated by the transmitted light intensity when the cavity was flushed with dry air. A.U., implies arbitrary unit. Bottom graph: Measured absorbance ($\ln(I_0/I)$) of methane and butane using the IBBCEAS set-up.

(Rohwedder et al., 2014). Hence, we tested the response of this BBCEAS system using a 1000 ppm and 873 ppm calibration mixtures of methane and butane respectively, in balance nitrogen manufactured by Gasco, US. To record the I_0 spectrum, the cavity was flushed with dry air every time before filling the cavity with the absorbing gas. The I spectra for methane ($I_{methane}$) and butane (I_{butane}) were measured by maintaining a continuous 0.1 liter per minute flow of the gases from the cylinders. The gases were introduced inside the cavity volume at ambient temperature (23^oC). Figure 6 shows the transmission signal through the cavity when flushed with dry air and absorbance measured from the experiments.

3.1.1 Conclusion

From the experiments conducted at EOL, it was found that this technique showed excellent response to the presence of methane and butane gas. Even at the minimum laser power and low concentrations, both the gases showed appreciable absorbance. This meant that a 75W tungsten-halogen bulb would be sufficient to obtain a reasonable dynamic range for the proposed NIR-IBBCEAS detector system. Since the expected absorbance values of ethane and propane would lie between that of methane and butane, we were able to conclude that the instrument was feasible for the detecting all four hydrocarbons. It should be noted that the conducted absorption measurements showcased the proof of principle and the results were qualitative. Since the gases were introduced at a low flow rate, the exact equilibrium concentration of the gases inside the cavity could not be estimated without the use of additional gas monitors or samplers. Hence, it was not possible to retrieve any quantitative information from the experiments.

However, as long as the main objective of testing the method's feasibility is concerned, it was found that the NIR-IBBCEAS instrumentation in the wavelength range of 1100-1250 nm has a

huge potential to serve as a sensitive detector for monitoring natural gas (methane, butane, ethane, and propane) leaks.

3.2 Spectrometer Calibration

Two of the main factors which decide the accuracy of concentration retrieval using the NIR-IBBCEAS instrument are utilizing the correct wavelength scale of the spectrometer and its spectral resolution. The spectrometer resolution must be determined to convolute the literature cross-sections to apply it to the measured spectrum. Hence, a proper spectrometer calibration procedure is necessary for performing the reliable quantitative analysis. The NIRez spectrometer's resolution and wavelength calibration were done using a Hewlett-Packard tunable laser source (HP 8168F) from the Quantum Cryptography and Communication Lab, Department of Physics, the University of Calgary headed by Dr. Wolfgang Tittel. The laser light was focused onto one end of an optical fiber through a neutral-density (ND) filter whose other end was attached to the entrance slit of the spectrometer to measure the laser peak. The ND filter was used to reduce the laser intensity to a moderate level to avoid spectrometer saturation. The wavelength of the laser peak was accurately measured up to 3 decimal places using a laser wavelength meter (621B-NIR from Bristol instruments). Four such laser peaks were measured between 900nm to 1700 nm wavelength range.

3.2.1 Spectrometer Resolution

In optical spectroscopy, resolution determines the minimum wavelength (or frequency) difference between two spectral peaks that the spectrometer can resolve. The resolution of the spectrometer can be obtained by fitting a Gaussian curve over the measured laser peak and

calculating its full width at half maximum (FWHM) (J. Chen, 2011). The Gaussian model used for the fit is given below.

$$I(\lambda) = c + be^{-\frac{(\lambda-m)^2}{2s^2}}, \tag{7}$$

Here, *c*, *b*, *m*, and *s* are the parameters to be fitted for with *s* being the standard deviation of the Gaussian curve. The FWHM of the fitted curve is then given by (Demtröder, 1971),

$$FWHM = 2s\sqrt{2 \times \ln(2)}, \tag{8}$$

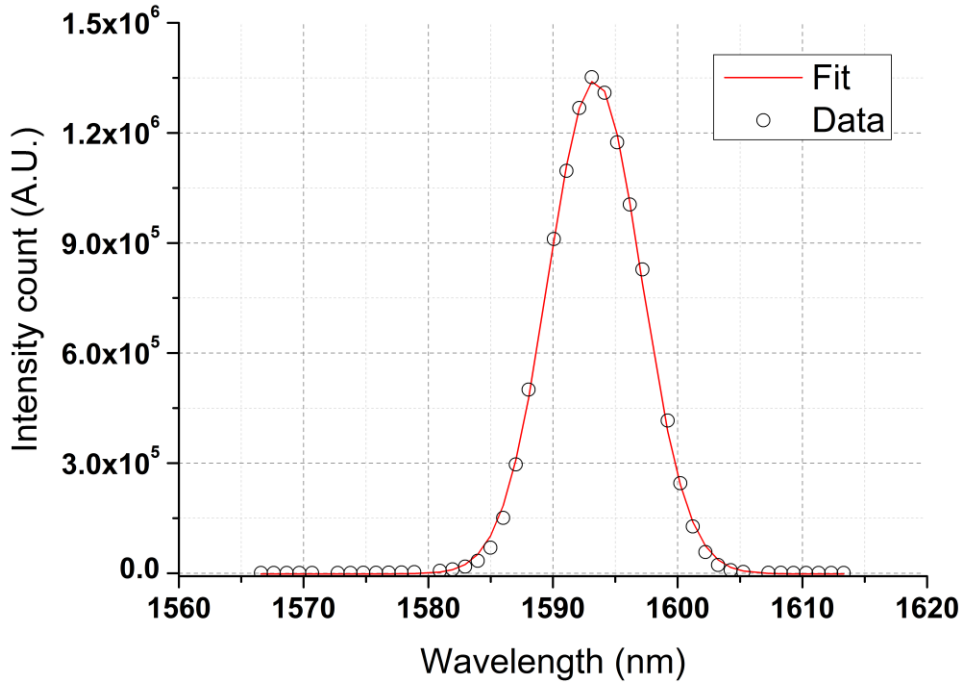

Figure 7: A Gaussian fit to the laser peak centered at 1591.436 nm showing a FWHM of 8.71 nm.

Figure 7 shows the Gaussian fit to the laser peak centered at 1591.436 nm. The fit deduced a spectrometer resolution of 8.71 nm. Performing such an operation on the other laser peaks yielded similar results.

3.2.2 Wavelength Calibration

In Figure 7, it should be noted that the wavelength of the laser peak recorded by the spectrometer was around 1593.12 nm instead of 1591.436 nm. Hence, it is evident that the wavelength scale of spectrometer requires calibration. The wavelength can be assigned to each pixel by fitting a second order polynomial to the pixel-wavelength mapping of the measured laser peaks.

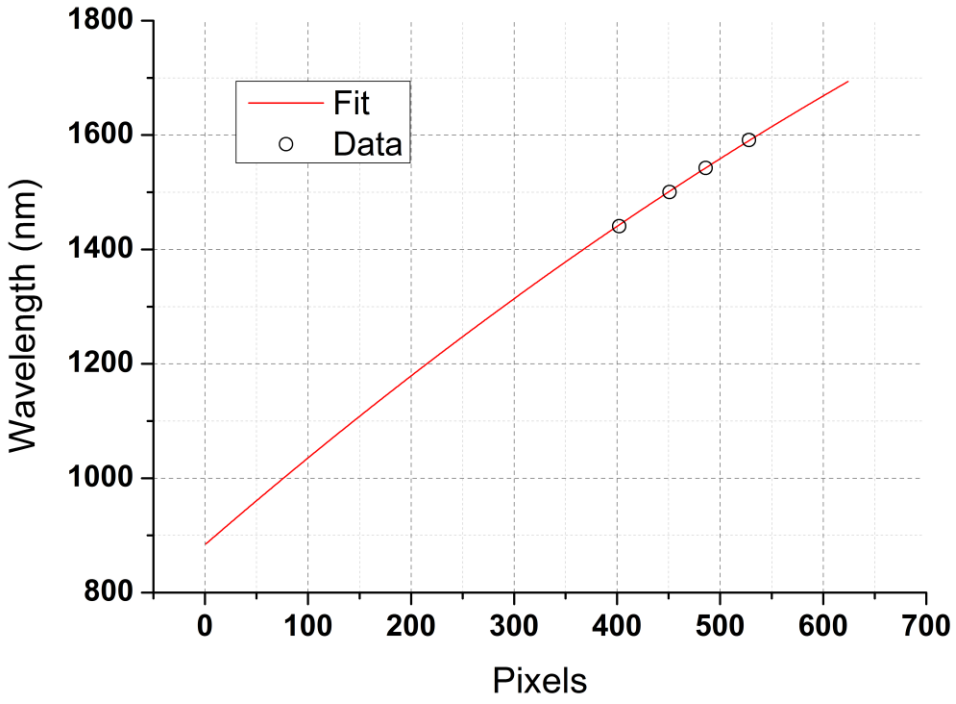

Figure 8: A second-order polynomial fit of the wavelengths to the pixels. Data represents the true wavelength of the laser peak and the pixel at which the spectrometer measured it. The fit obtained an absolute error of 0.8 nm for the difference between the true and calibrated wavelength.

The fit equation is given below.

$$\lambda_p = a + bp + cp^2, \quad (9)$$

In the equation above, λ_p denotes the wavelength of pixel p with a, b and c denoting the fit coefficients. The fitting was performed using the true wavelength values measured by the laser wavelength meter and the pixel number of the corresponding peaks observed in the spectrometer. A second-order linear regression was performed on these data, and the results are shown in Figure 8. The analysis produced an R square value close to 1 (0.9998).

3.3 Reference Cross-section Generation

From equations 2 and 3, it is apparent that one must know the absorption cross-section of absorbing gases to conduct qualitative and quantitative (number density) detection. Except for methane, absorption cross-section of no other hydrocarbons under consideration is available in the literature for the spectral range of 1100-1250 nm. Hence, the absorption cross-section values of butane, ethane, and propane were measured in the instrument's resolution using an IBBCEAS configuration. The measurement was carried out in the Applied Optics & Instrumentation Lab, Department of Physics, National Institute of Technology Calicut (NITC), India. The IBBCEAS system installed is depicted in Figure 9.

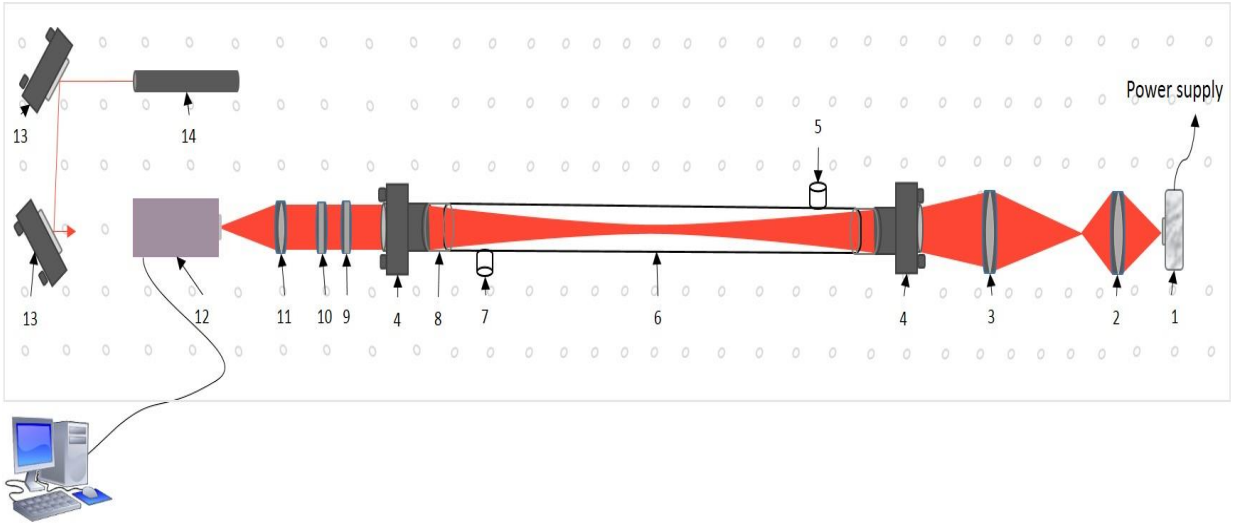

Figure 9: Schematic diagram of the IBBCEAS set-up for cross-section measurements. 1, Xenon lamp; 2, 2" lens (f=3 cm); 3, 2" lens (f=6 cm); 4, highly reflective cavity mirror; 5, gas inlet; 6, PVC pipe; 7, gas outlet; 8, vacuum bellow; 9, long pass filter (1100nm); 10, short pass filter (1250 nm); 11, 1" focusing lens (f= 6 cm); 12, NIRez Spectrometer; 13, Aluminium mirror; 14, He-Ne laser (red).

The set-up uses a 300 W CeraLux ceramic xenon short arc lamp (Luxtel, Inc.) as the light source along with the Layertec cavity mirrors and NIRez spectrometer purchased for the NIR-IBBCEAS detector. The 100 cm long optical cavity was closed using a 1" diameter PVC pipe with an inlet and outlet to facilitate gas flow. Vacuum bellows were also used to reduce disturbances on cavity mirrors during the gas flow. A He-Ne laser was used to align the optical resonator. The entire set up was installed on the top of an optical breadboard table.

3.3.1 Reflectivity Calibration

It was observed that methane has an absorption feature on the first half of the 1100-1250 nm wavelength range (Figure 6). Similarly, carbon dioxide has a weak absorption feature on the latter half of 1100-1250 nm wavelength range. The absorption cross-section of both gases in this wavelength region is available in HITRAN database. Hence, using known concentrations of both gases, wavelength dependent reflectivity of the mirrors could be determined using equation 4. But at first, the high-resolution cross-section data obtained from HITRAN was convoluted to the instrument resolution of 8.71 nm (Figure 10).

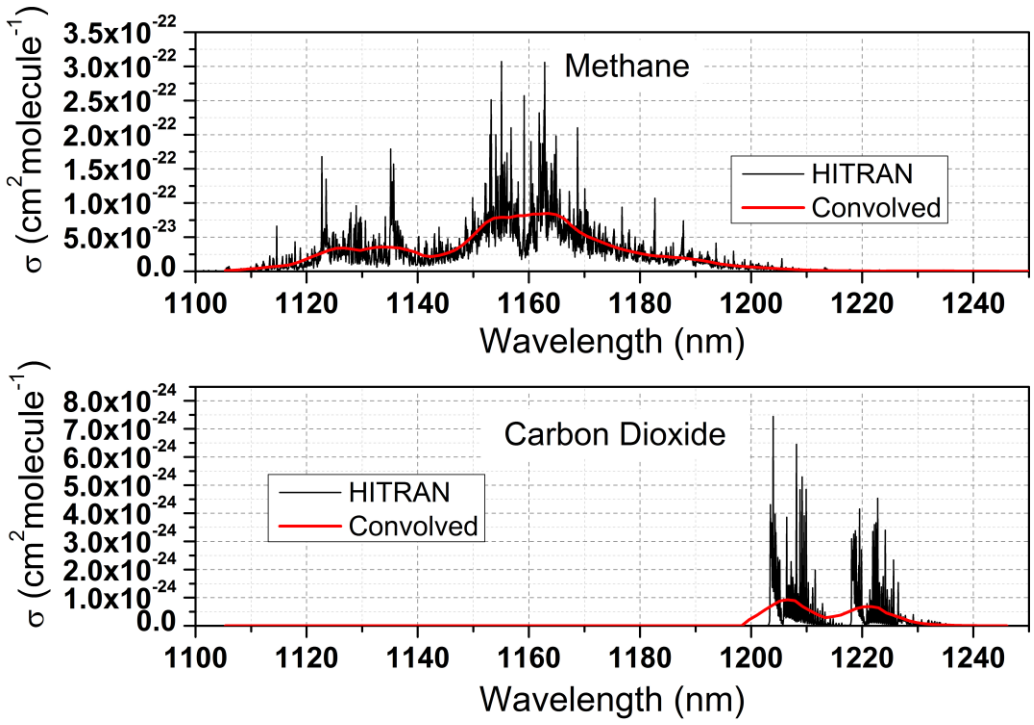

Figure 10: Convoluted and high resolution HITRAN cross-sections of methane and CO_2.

Reflectivity calibration was conducted using 1090 ppm methane and pure (99.99%) carbon dioxide gas. The absorbance due to both these gases was measured by introducing them separately inside the cavity volume at ambient pressure and temperature (P=1 atm and T=23^{o}C). Before and after the gas measurements, the cavity was flushed with nitrogen to measure the I_0 spectrum. Spectrometer's dark signal (I_{dark}) was recorded by covering the light source completely. The spectra were recorded by averaging ten scans with an acquisition time of 1 second and a gain of 64 (maximum value). The NIRez spectrometer software gave limited user control on setting the measurement parameters. The integration time was a fixed quantity which cannot be changed by the user. Hence, an improvement in signal intensity values cannot be achieved as it depends on increased acquisition time. The measured I, and I_0 spectra were dark

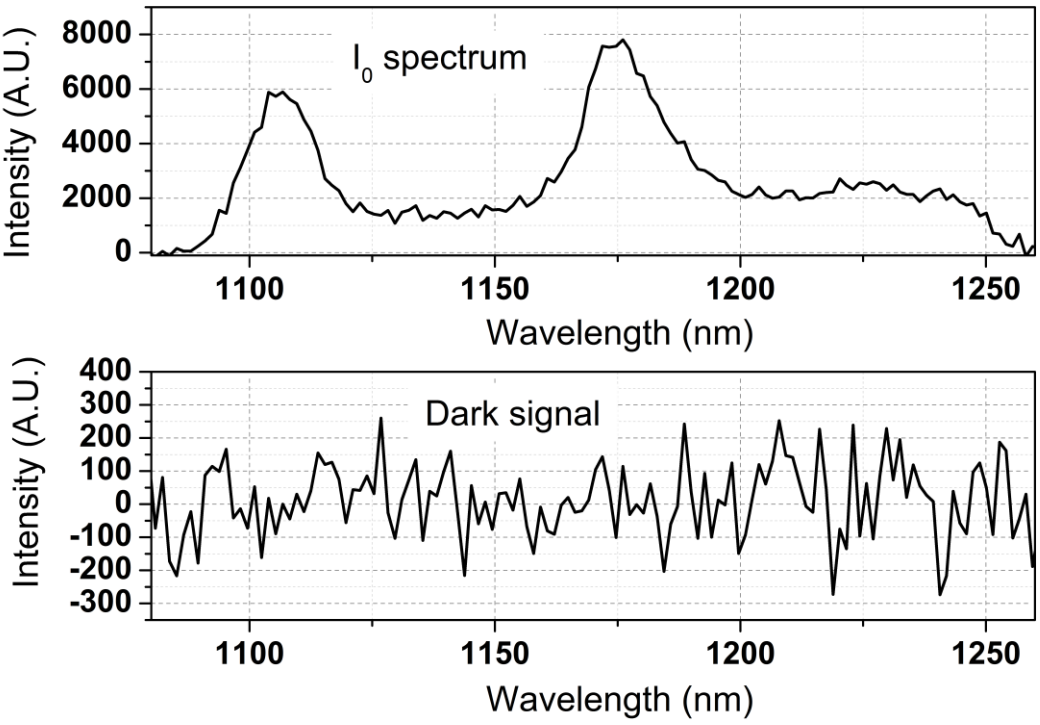

Figure 11: Top curve: A typical I_0 spectrum measured using the Xenon lamp. Bottom curve: Dark spectrum obtained by blocking the source.

corrected, by subtracting the I_{dark} from them, before calculating the absorbance. Figure 11 shows a sample reference signal (I_0) and dark spectrum.

The measured absorbance in conjunction with the convoluted cross-sections and equation 4 were used to determine the wavelength dependent reflectivity of the cavity mirrors. The number density was calculated using the ideal gas law. The R(λ) values were further interpolated and fitted using a second order polynomial. The obtained mirror reflectivity is shown in Figure 12. The error was found using the standard deviation of measured value from the fit.

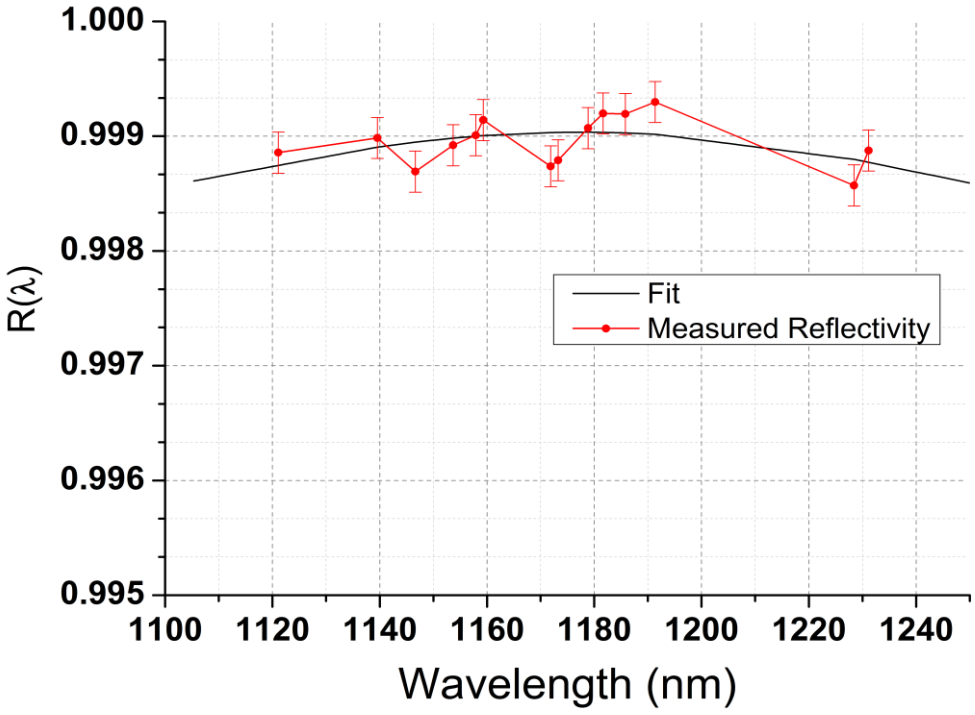

Figure 12: The experimentally determined reflectivity as a function of wavelength in the 1100-1250 nm range for absorption cross-section measurement experiments. The solid line represents a second-order polynomial fit to the reflectivity values (dotted-line curve). The error bars indicate a one standard deviation of ± 0.00018 (fit uncertainty) from the fit.

3.3.2 Absorption Cross-section Measurements

Absorption cross-section of a gas can be calculated with knowledge of gas concentration inside the cavity volume, reflectivity, cavity length and its IBBCEAS absorbance. By re-arranging equation 4, the mathematical expression for absorption cross-section is obtained as,

$$\sigma(\lambda) = \frac{\left(\frac{I_0(\lambda)}{I(\lambda)} - 1\right)\left(1 - R(\lambda)\right)}{nL}, \tag{10}$$

The terminologies and units for equation 10 remain the same as equation 4. To determine the absorption cross-sections of butane, ethane, and propane in the wavelength region of 1100-1250 nm, their IBBCEAS absorbance through the 100 cm long optical cavity was measured. The concentrations of the gases used were 1003 ppm butane, 998 ppm ethane and 1007 ppm propane which were introduced separately at ambient conditions mentioned earlier. Transmission spectra of nitrogen gas-filled cavity volume were used as I_0 spectra. All the spectrometer parameters from section 3.3.1 were retained along with dark correction procedure. The absorbance data along with the calibrated reflectivity were applied in equation 10 to calculate the absorption cross-section values. These values were fitted in Origin using the multiple peak fitting technique assuming a Gaussian model. The computed absorption cross-section data of butane, ethane, and propane are illustrated below in Figure 13.

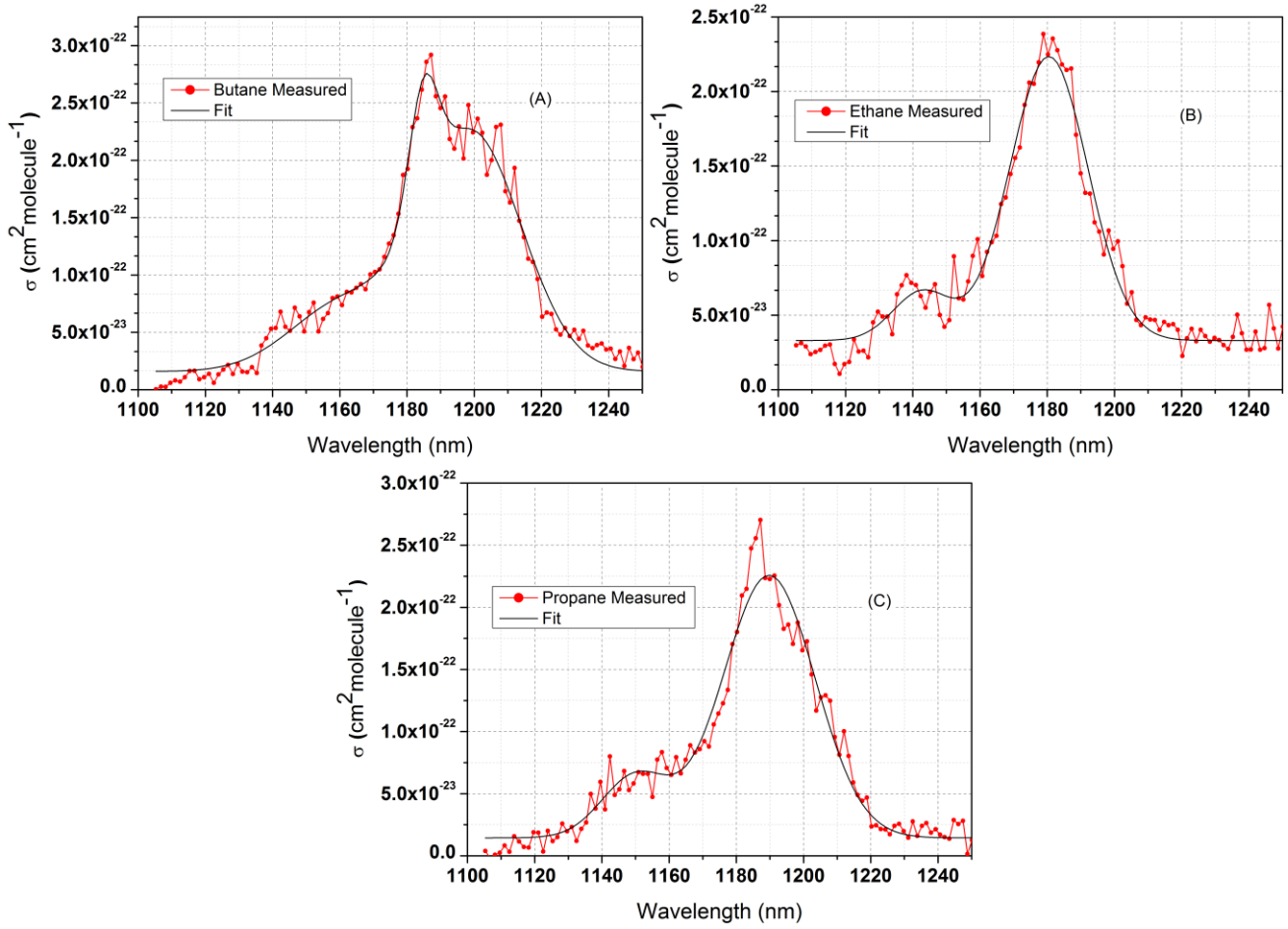

Figure 13: The reference absorption cross-section of (A) butane (R^2=0.977), (B) ethane (R^2=0.965) and (C) propane (R^2=0.962), determined using the NIR-IBBCEAS instrument.

3.4 Summary

A broadband CEAS system was developed for performing a qualitative testing on the applicability of the proposed wavelength range for detecting methane, butane, ethane, and propane. Based on the measured absorption of methane and butane, it was demonstrated that the technique was feasible for the detecting all four hydrocarbons employing the wavelength range of 1100 to 1250 nm. Before setting up the NIR-IBBCEAS system, the spectrometer was also wavelength calibrated along with determining the spectrometer resolution. Further, the

absorption cross-section values of butane, ethane and propane had to be measured individually as they were not available in the literature. This was performed by installing an IBBCEAS arrangement and filling the closed cavity with known amount of these gases.

Chapter 4: NIR-IBBCEAS Instrumentation

After successfully verifying the proof of principle and performing the required lab measurements and calibrations, the plot was set to develop this technique into a compact and portable instrument which could be deployed in industrial facilities. In this section, the instrumentation, performance study and software development of the NIR-IBBCEAS natural gas leak detector is discussed in detail.

4.1 Instrument Set-up

The initial idea was to use the same configuration described in Figure 9 (installed for measuring the cross-section at NITC) for building the detector. The only change expected was to replace the xenon lamp in the figure with the tungsten-halogen light source bought for the instrument. Apart from the radiance benefits discussed in section 2.3.1, the tungsten-halogen source from Spectral Products had added benefits of lower heat generation and improved in-house cooling compared to the xenon lamp at NITC. However, some initial testing done with this showed that it was difficult to align and couple the light from the tungsten-halogen lamp into the optical cavity using this configuration. Hence, the arrangement portrayed in Figure 14 was adopted to build the NIR-IBBCEAS natural gas leak detector. The additional aluminum-coated mirrors used between the source and cavity mirror (components 3 and 4 in Figure 14) provided a better spatial (horizontal and vertical) control over the light beam for resonator alignment. The choice of focusing optics near the source (components 2, 5 and 6 in Figure 14) was also based on the initial testing to efficiently couple the broadband light into the optical cavity. A 635 nm red diode laser

module was employed for aligning the optical cavity and light source. This was cheaper and readily available than the He-Ne laser used earlier in cross-section measurements.

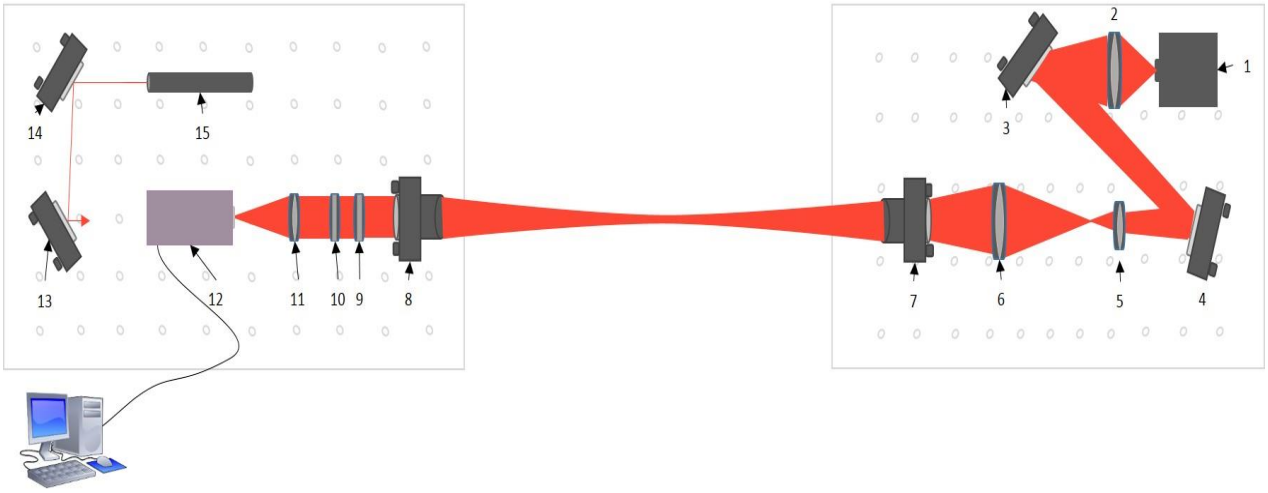

Figure 14: Schematic diagram of the NIR-IBBCEAS instrument. 1, Tungsten-Halogen Light source; 2, 2" lens (f=6 cm); 3,4,13,14 Aluminum-coated mirror; 5, 1" focusing lens (f= 2.5 cm); 6, 2" lens (f=7 cm); 7, 8, highly reflective cavity mirror; 9, long pass filter (1100nm); 10, short pass filter (1250 nm); 11, 1" focusing lens (f= 6 cm); 12, NIRez Spectrometer; 15, Alignment laser.

4.1.1 Structural Design

The key features considered while designing the structural framework of this instrument were (i) the mechanical stability, (ii) portability and mobility and (iii) the ease of sample diffusion into the cavity volume. These are some of the important factors which decide its applicability in an industrial space monitoring gas leaks.

Mechanical stability of the external framework and instrument platform is important to reduce the effects of immediate environment on the system alignment and performance. The system should be strong enough to withstand small external disturbances but also light enough to reduce the overall weight of the instrument to make it portable. Hence, T-slotted aluminum framing extrusions (40 mm*40 mm) were used to build the supporting framework to house the

instrument. The structure was built by joining the extrusions using M5 socket head cap screws and hammer T aluminum connector nuts. This provided flexibility of making dimensional adjustments based on the size of optical components and breadboard. In order to support its movability and to obtain an accessible and efficient sampling volume, the instrument was divided into separate enclosed transmitter and receiver units (Figure 14). The source, focusing optics and one of the cavity mirrors formed the transmitter unit while the receiver unit comprised of the second cavity mirror, filtering and focusing optics, spectrometer and the alignment laser. Hence, two hollow cuboidal arrangements (dimensions of (a) receiver box: 18.5” * 13” * 15.5” and (b) transmitter box: 20” * 11.5” * 15.5”) covered with aluminum composite panel (ACP) sheets on all the sides (Figure 15) were built to house both the units. Rubber bushes were attached at the cuboidal base to minimize vibrational effects. The hollow box-like structures, within which the optical breadboards were installed, were connected using rails of length 50 cm, adjustable up to a maximum of 100 cm.

Figure 15: The supporting structural framework for housing NIR-IBBCEAS instrument. The separation between the transmitter and receiver units could be varied from 50 cm to 100 cm.

The covering sheets were removed while setting-up the instrument and closed afterward for a tidy and compact look.

4.1.2 Light Source

The light source from Spectral Products was housed in a bulky metal box (Figure 16) which contained the tungsten-halogen lamp (bulb with focusing optics), cooling fan and the electronics panel. Integrating this entire box inside the transmitter unit was not possible. Hence, the parts were dismantled from the box and arranged more efficiently inside the NIR-IBBCEAS instrument.

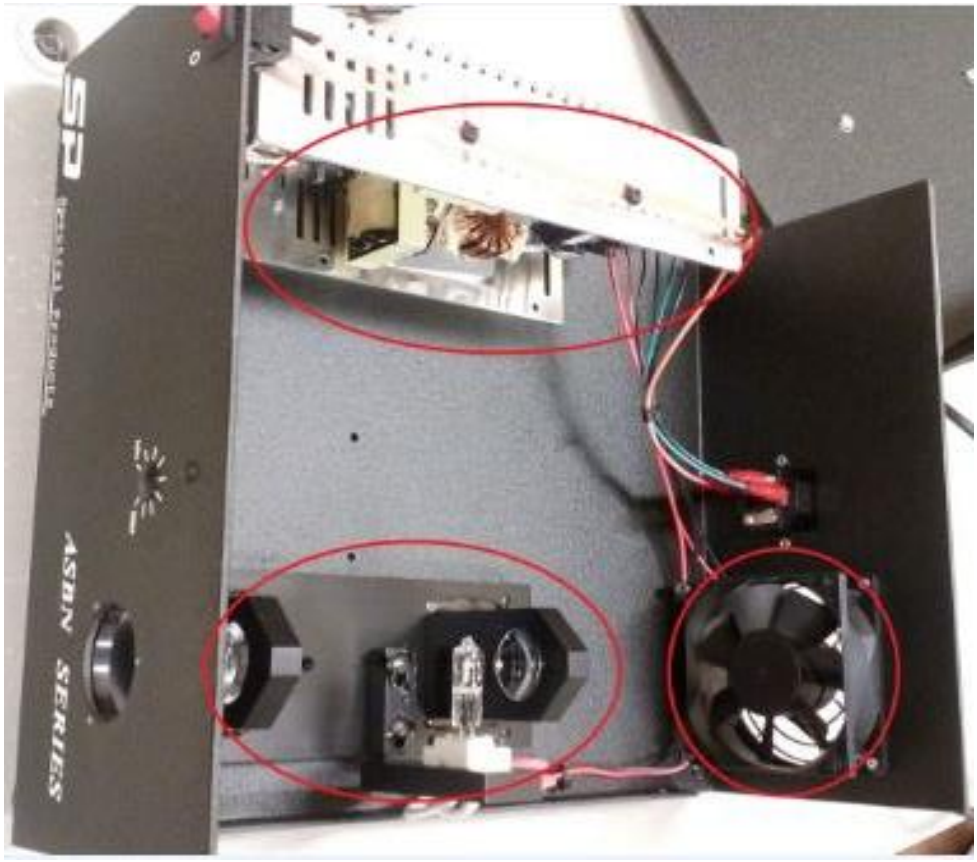

Figure 16: Inside view of Spectral Products tungsten-halogen light source. The circled portions are the lamp (bulb and focusing optics), cooling fan and electronics unit.

The average optical height of the set-up, which is decided by the height of alignment laser beam, was fixed at 102 mm from the breadboard surface. This implies that the center of all the involved optical components (lenses, mirrors, and filters) and tungsten-halogen bulb should be placed 102 mm high. Optical components were brought to this height using optical posts. However, to raise the source, a platform was designed in SolidWorks and machined at the University of Calgary machine shop. The details of the design are given in the appendix. The platform along with the source was then fixed on the breadboard inside the transmitter unit.

Light source is a key component in an IBBCEAS system. Hence, fluctuations and long-term drift in lamp intensity can affect the measured extinction coefficients. These parameters were

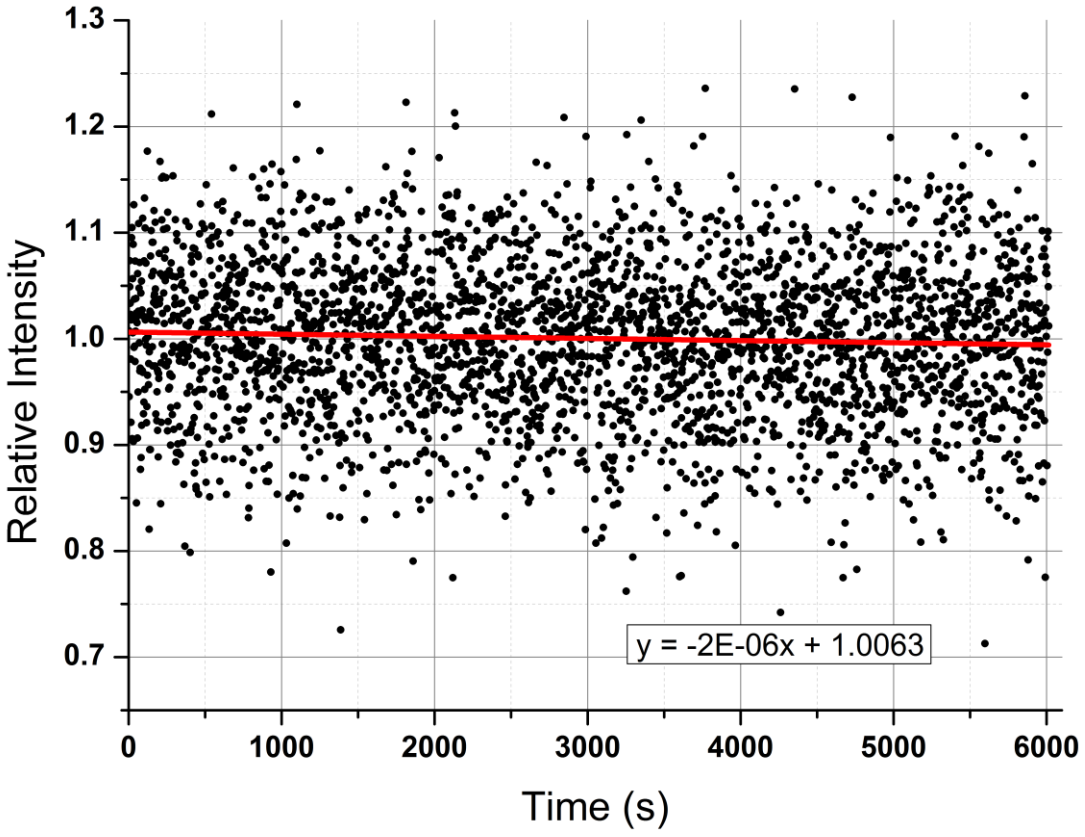

Figure 17: The temporal dependence of tungsten halogen lamp intensity at 1240.64 nm. Long term drift was calculated from the slope of the trend line as 0.72% per hour. Short-term fluctuation is approximately 7.2%.

analyzed using spectra collected for about 2 hours with the spectrometer using a 1 second integration time. The results based on the intensity at 1240.64 nm are shown in Figure 17. The lamp output was fairly stable over a long time with a dimming of 0.72% per hour while the short-term fluctuations were around 7.2% (one standard deviation from the trend line). The effect of long-term drift on the measured extinction coefficient is negligible for the results presented in this thesis since the duration of all experiments were less than an hour. However, for continuous long-term monitoring applications of this system, it can result in an appreciable error in the retrieved concentrations. For e.g., if I_0 was measured 5 hours before a particular I spectra, it could cause an error of about 4% in the calculated extinction coefficient. Hence, in order to safely ignore the error due to long-term intensity drift on the retrieved gas concentrations, it would be advisable to measure I_0 after every two hours at least. On the other hand, the short-term fluctuations can result in huge errors in the retrieved concentrations along with decreasing the sensitivity of the detector. This can be improved by averaging multiple spectra. Optimum number of spectra to be averaged and the errors resulting from the averaged spectra are discussed later in the thesis.

4.1.3 Instrument Assembly and Cavity Alignment

Aligning an optical cavity for a broadband source is trickier than for a laser source. Hence, the process should be done with extreme care. In this case, even though the optical cavity was employing a broadband source, its alignment was achieved using a 635 nm red diode laser. The resonator alignment process is discussed below.

Once the breadboards were fitted inside the extrusion framework, the red laser was installed in the receiver end. The laser beam height was set at 102 mm, and the light was directed towards

the transmitter end using aluminum-coated mirrors, as shown in Figure 14. Using the adjuster knobs of the kinematic mirror mounts, a straight laser beam parallel to breadboard surface (102 mm above the surface) was achieved. Then, the tungsten-halogen lamp with its platform (section 4.1.2) was fixed inside the transmitter unit along with its cooling and electronic panels. The light from the lamp was made to track the laser beam path backward towards the diode laser using the two aluminum-coated mirrors in the transmitter end. Using the adjuster knobs of these mirrors, the broadband light was made concentric to the laser beam and follow the same optical path as that of the laser, but in the opposite direction. After that, the lenses 2, 5 and 6 from Figure 14 were introduced to focus the broadband light. The separation between lenses 5 and 6 was adjusted to obtain a sharply focused broadband light at the center of cavity volume, which diverges afterward. In the next step, one of the cavity mirrors was placed on the transmitter side, and the broadband source was switched off. Since the cavity mirror was concentrically placed in the laser beam path, a portion of the incident laser beam would be reflected while the rest would be transmitted through the mirror. Using the adjuster knobs of the cavity mirror holder, the reflected beam was made colinear to the incident ray to track the path back to the laser. This was followed by positioning the second cavity mirror concentrically with the laser path in the receiver unit at a separation of 60 cm from the first cavity mirror. Similar to the previous step, the reflected light from the second mirror was made collinear with the incident laser beam. Then, the broadband source was switched on, and the filters, focusing lens, and the spectrometer were installed in the receiver end. The spectrometer was connected to the computer via USB and cavity signal was measured using the spectrometer software. Finally, minute adjustments were performed in the adjuster knobs of the cavity mirror holders to maximize the signal intensity. The cavity signal obtained is shown in Figure 18. The peaks (~1030 nm, 1633 nm, and 1686 nm)

obtained outside of the designated NIR range (1100-1250 nm) may be due to the imperfections in the low and high pass filter coatings.

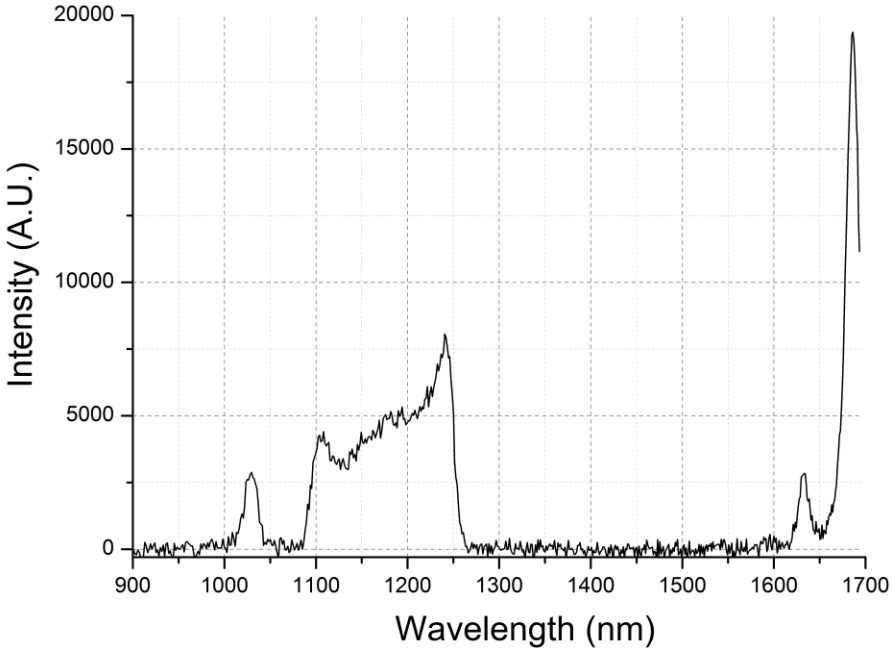

Figure 18: A typical cavity signal obtained for a properly aligned NIR-IBBCEAS gas detector with a gain of 64.

To perform reflectivity calibration and gas testing experiments, the 60 cm cavity length was closed using a PVC pipe with an inlet and outlet for facilitating the gas flow. Vacuum bellows were also used on both ends to reduce disturbance on the mirrors due to gas flow. The assembled NIR-IBBCEAS natural gas detector prototype is shown in Figure 19.

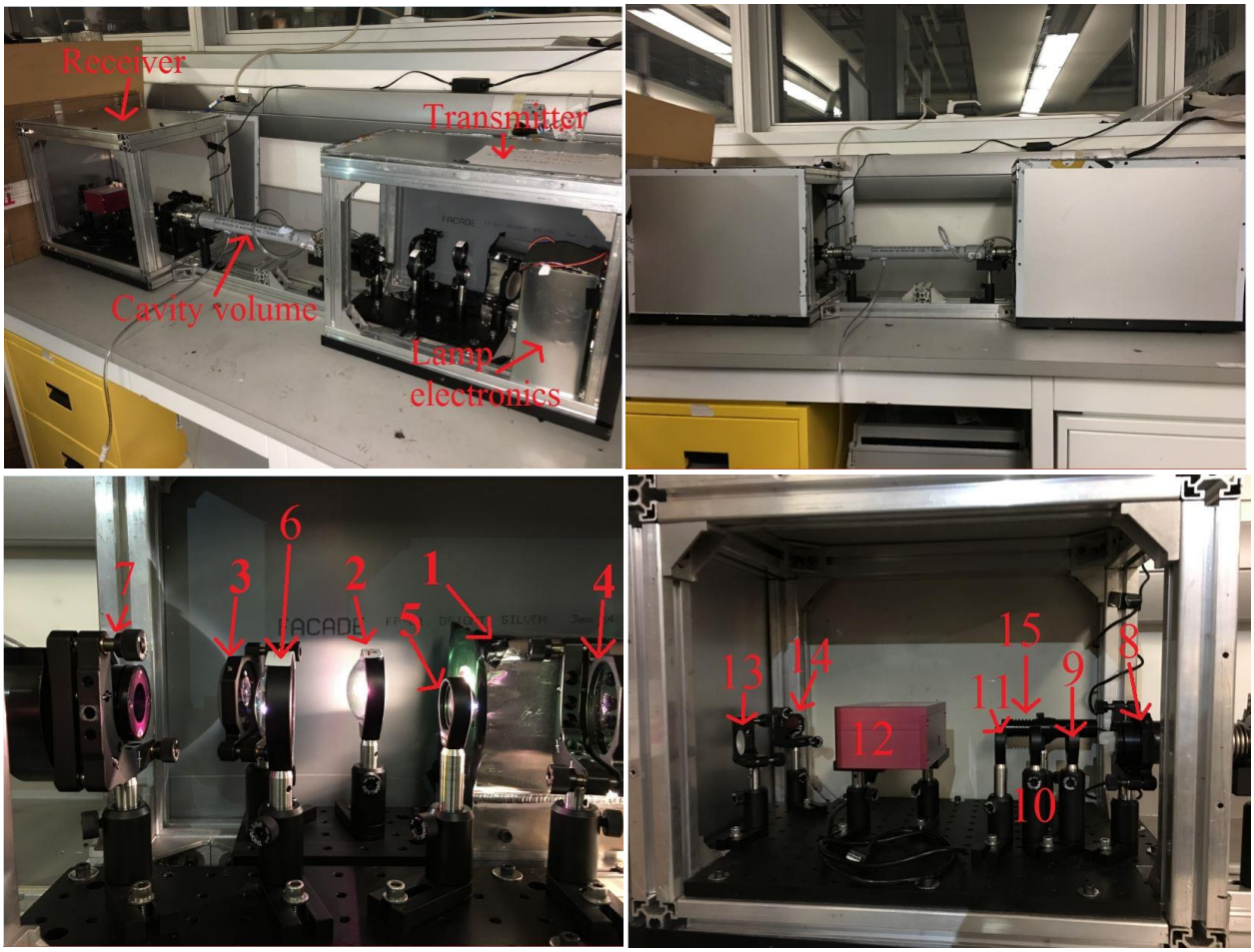

Figure 19: The working prototype of NIR-IBBCEAS natural gas detector developed for the current study. The figure on the bottom left shows the inside view of transmitter unit and the bottom right figure depicts the receiver unit. The numbering is based on Figure 14.

4.2 Instrument Stability and Allan Variance

Stability of the instrument is an important factor to be considered for instruments dealing with sensitive detections. In an ideal world, the stability of instrument is wholly limited by random noise (white noise) which in principle, could be reduced by increasing the signal averaging. Generally, signal averaging increases the signal to noise ratio (SNR) by a factor of $N^{1/2}$ where N denotes the number of spectra averaged (Burdett, 2005). However, in the real-world scenario, due to other inevitable noises such as source fluctuation, spectrometer stability, and systematic signal drifts, there exists an optimal averaging point beyond which the SNR will not improve further. Allan variance is a statistical tool to determine this optimal point which results in the maximum sensitivity (Medina, 2011; PO Werle et al., 1993; T Wu et al., 2012; Tao Wu et al., 2009).

Estimation of the NIR-IBBCEAS detector's stability and optimum averaging time was carried out by applying Allan variance study on the IBBCEAS spectra within the 1100-1250 nm range. The cavity was flushed with nitrogen, and transmitted intensity of the cavity signal was registered for 230 consecutive 1-second spectra (without any averaging). It should be noted that the integration time of 1 second is a fixed value for the spectrometer. The following procedure was adopted to calculate the Allan variance (J. Chen, 2011):

The intensity values in every pixel from all the 230 (N) spectra were used to create a matrix Y with each element in the matrix of the form $Y_{p,\,n.}$ The index p denotes the pixel number within the mirror range (1100 to 1250 nm) while n denotes spectra (n=1, 2, …N). Then, the N elements were divided into M groups containing K data points. Within each group, the data points were averaged as below,

$$X_{p,i}(K) = \frac{1}{K}\sum_{m=1}^{K} Y_{p,ik+m,} \quad i = 0,1,\dots,M; M = \frac{N}{K} - 1 \tag{11}$$

These averages were used to determine the Allan variance of each pixel by the following equation.

$$\sigma_A^2(p,K) = \frac{1}{2M}\sum_{i=1}^{M}\left(X_{p,i+1}(K) - X_{p,i}(K)\right)^2, \tag{12}$$

The averaged Allan variance of all the pixels were calculated by,

$$\overline{\sigma_A^2(K)} = \frac{1}{P}\sum_{p=1}^{P}\sigma_A^2(p,K), \tag{13}$$

with the bin size, *K* varied from 1 to 115 (*N/2*). Averaging time is then given by,

$$\tau = K \times t_0, \tag{14}$$

where t_0 in our case is 1 second. The log-log plot of averaged Allan variance as a function of averaging time (τ) is given in Figure 20. From the Allan plot, the optimal averaging time was found to be around 75 seconds (minimum of the plot), beyond which averaging does not improve the SNR. The plot also depicted a local minimum at around 30-second region indicating good SNR characteristics. For gas-based quantitative experiments, higher averaging time implies more

gas usage. Moreover, the gain in SNR from 30 to 75 seconds is quite small compared to the gain from 1 to 30 seconds. Hence, considering the experimental benefits and simplicity, for the results presented in the thesis, the averaging time was chosen to be 30 seconds (i.e., averaging 30 spectra with 1 second integration time), which is slightly below half the optimum averaging time.

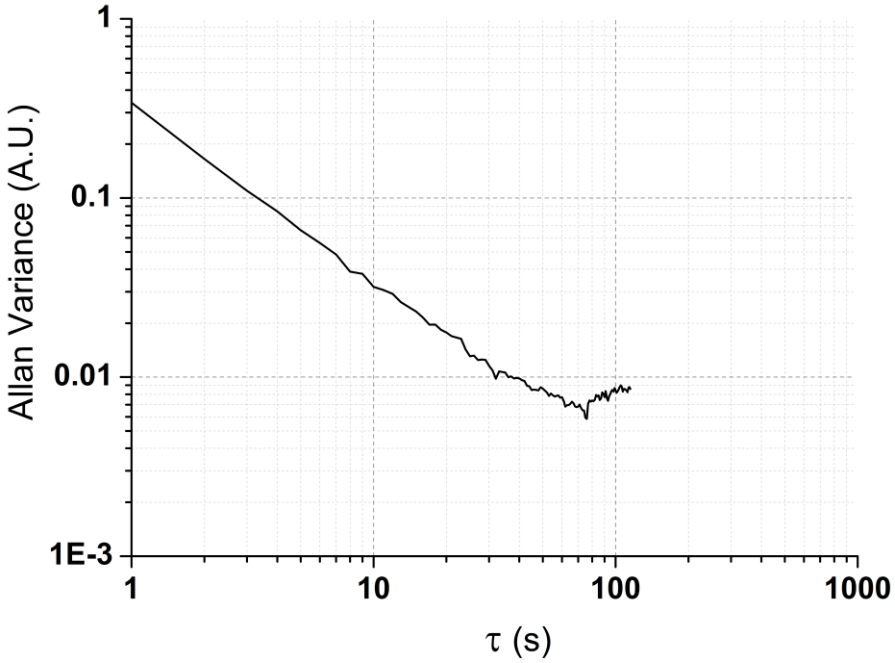

Figure 20: A log-log plot of Allan variance as a function of averaging time for the mirror wavelength. At τ = 75 s, Allan variance showed a minimum, indicating maximum SNR.

4.3 Software Development

A user-friendly software package was developed in LabVIEW platform to automate the NIR-IBBCEAS working. As mentioned earlier, due to the limited user-control of NIRez spectrometer software, neither the save directory of the spectrum measurement could be changed from its default nor does it have a LabVIEW library to control it. Hence the data logging portion of the program copied the spectrum from its default folder and moved it to the working folder every time a measurement was made. The pre-requirements of the program are the mirror reflectivity

(in .txt format), absorption cross-section of gases (in .txt) and cavity length employed (see Appendix).

The software could be run in three modes: Data collection and Analysis, Data collection only and Post analysis only. In the first mode, the program follows a sequential routine of collecting dark, I_0 and I spectra where it prompts the user to confirm the transition between each type of spectrum. As soon as the first I spectrum is recorded, a real-time quantitative analysis of the measured spectra is carried out in parallel with the data collection. The analysis is based on a singular-value decomposition (SVD) technique based on linear least square approach. The fitting procedure is discussed in detail in Chapter 5. The real-time concentration of each of the gases (methane, ethane, propane, and butane) are shown in a time series with a choice of display units between ppm, ppt, and ppb. The user could also change the detection scheme to any of the individual gases or other combinations of these gases. Apart from the spectra, the program also saves the time-series concentration of the gases along with its fitting uncertainty, fit curve and fit residuals to the working directory. In the Data collection only mode, the data logging is the only process taking place where I_{dark}, I_0 and I spectra get saved to the working directory following the sequential routine mentioned earlier. The analysis of such data could be carried out at a later time using the Post analysis mode of the software. The program also has an optional feature of performing a normalization procedure to correct the intensity fluctuations of the light source. This is done by monitoring the intensity changes of a non-absorbing wavelength with respect to the first I spectrum recorded and scaling intensity of all other wavelengths using these scaling factors.

The software almost completely automates the instrument into a real-time monitoring detector without the need for user intervention or inputs once started. Figure 21 depicts the front panel of

the program containing separate interchangeable tabs for displaying spectrum collection, SVD

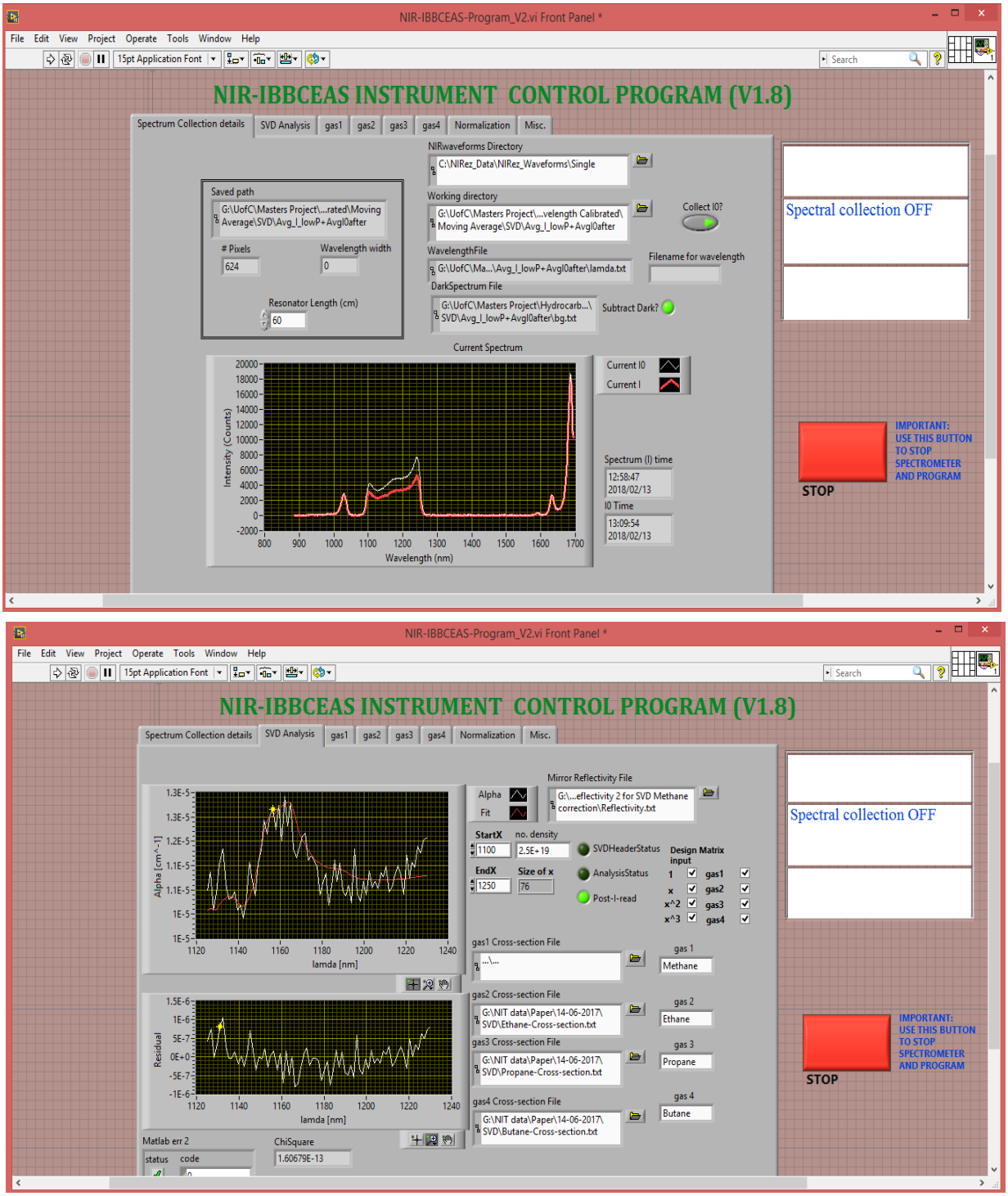

Figure 21: The user interface of the NIR-IBBCEAS automation software. The plots displayed are for 995.1 ppm methane detection. Top figure corresponds to spectrum collection while the bottom figure displays the SVD fitting.

analysis, gas concentrations and normalization details.

4.4 Summary

The NIR-IBBCEAS detector system was aligned and installed on an aluminum extrusion framework. The lamp fluctuation and intensity drift were studied, and the light source intensity was found to be fairly stable. Instrument stability was also analyzed using Allan variance and the optimal averaging time was found to be 75 seconds. However, considering experimental benefits, 30 seconds was fixed as the average time. Further, a user interface for automating the process of measurements and quantification was developed in LabVIEW platform. Utilizing all these, the instrument was prepared for performing gas testing.

Chapter 5: Experiments and Analysis

After setting up the NIR-IBBCEAS natural gas detector, the instrument was tested with a methane sample and a hydrocarbon mixture of methane, butane, ethane, and propane in a closed cavity configuration. This chapter details these experiments and results along with information on the spectral analysis procedure and reflectivity calibration.

5.1 Reflectivity Calibration

The cavity mirrors used in the instrument remained the same from the absorption cross-section measurement experiments. Even though the reflectivity of the mirrors was measured then, it is important to calibrate the mirror reflectivity every time the IBBCEAS cavity is aligned. This is due to effects of factors such as environmental changes, dust deposition, mechanical disturbances and alignment differences on the mirror performance. Since the high reflectivity of such mirrors can show appreciable differences with the broadness of wavelength range, the reflectivity calibration is important for absolute absorption measurements in IBBCEAS (Ruth, Dixneuf, & Raghunandan, 2014).

Like earlier, the wavelength dependent reflectivity of cavity mirrors was determined using a known amount of methane and carbon dioxide gas along with their convolved absorption cross-section values. The exercise was carried out using 4.971% methane and 99.99% carbon dioxide by volume, supplied by Praxair Inc, Canada. I_0 spectrum was measured by flushing the cavity with nitrogen gas before filling the cavity with an absorbing gas. The gases were introduced at 1 atm pressure and ambient temperature (23^{o}C). The transmitted spectrum of the absorbing sample was measured by separately passing methane (I_{CH_4}) and carbon dioxide (I_{CO_2}) through the closed

cavity. The dark spectrum (I_{dark}) was recorded by blocking the light source completely. All the spectra were recorded with a gain of 64 and an integration time of 1 second by averaging 30 consecutive scans. The measured I (I_{CH_4} and I_{CO_2}), and I_0 spectra were dark corrected, by subtracting the I_{dark} from each of them. These data along with the convolved cross-section values (Figure 10) and cavity length (60 cm) were applied in equation 4 to calculate the mirror reflectivity. The calculated reflectivity values were further interpolated and fitted using a second-order polynomial. The result is shown in Figure 22. The error was determined using the standard deviation of measured value from the fit.

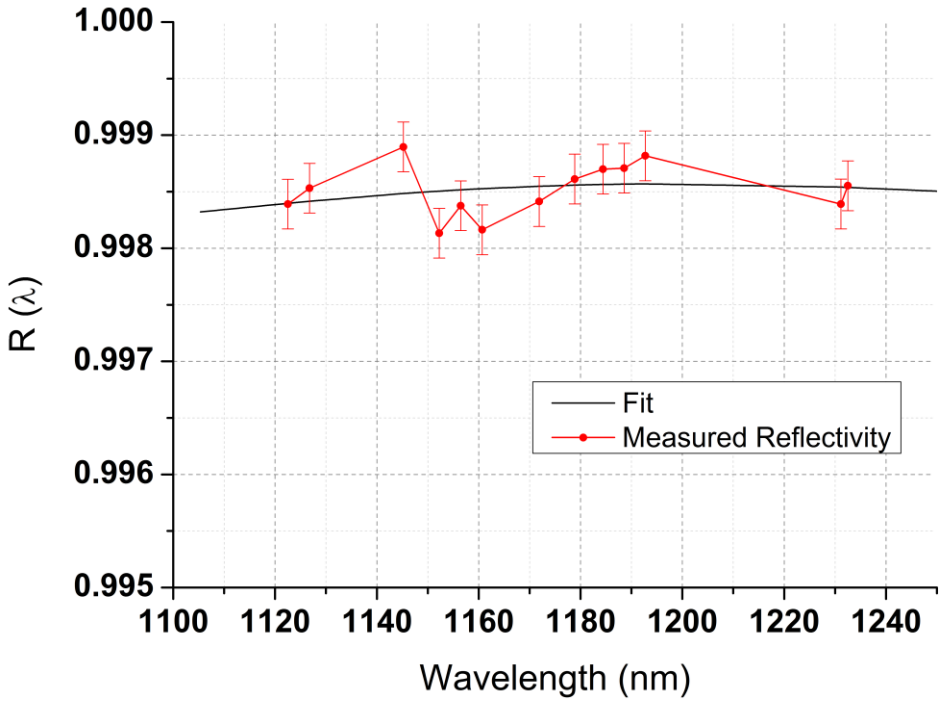

Figure 22: The experimentally determined reflectivity of the NIR-IBBCEAS detector instrument in the 1100-1250 nm range. The solid line represents a second-order polynomial fit to the calculated reflectivity values (dotted-line curve). The error bars indicate a one standard deviation of ± 0.00022 (fit uncertainty) from the fit.

5.2 Data Analysis

Simultaneous multiple gas quantification requires a standard procedure to retrieve the concentration of each species from an experimentally measured absorption (or extinction) spectrum of the mixture. This is due to the highly overlapping rotational-vibrational absorption bands of hydrocarbons in this wavelength regime.

5.2.1 Spectral Fitting

Recalling equations 2 and 3, the measured absorption (or extinction) coefficient occurring from gas-phase absorption can be expressed as,

$$\alpha(\lambda) = \frac{1}{L}\left(\frac{I_0(\lambda)}{I(\lambda)} - 1\right)\left(1 - R(\lambda)\right) = \sum_i \sigma_i(\lambda) \int_0^L n_i(x)dx, \qquad (15)$$

All the terms have the same meanings as mentioned in equations 2 and 3. This implies that knowing the absorption cross-section values of the components, their number density can be retrieved from measured absorption by applying a fitting routine on equation 15.
However, in the real world, apart from the molecular absorption, light extinction can happen due to additional unspecified background activities such as aerosol scattering and extinction due to fluctuations of lamp intensity. Hence, the number density of individual components was retrieved by performing a linear least square spectral fitting on the measured extinction coefficient by expressing it with the following equation,

$$\alpha(\lambda) = a + b\lambda + c\lambda^2 + d\lambda^3 + n_{CH_4}\sigma_{CH_4}(\lambda) + n_{C_2H_6}\sigma_{C_2H_6}(\lambda) + n_{C_3H_8}\sigma_{C_3H_8}(\lambda) + n_{C_4H_{10}}\sigma_{C_4H_{10}}(\lambda), \quad (16)$$

where *n* represents the number density [molecule cm^{-3}], σ denotes the reference absorption cross-section [cm^2 $molecule^{-1}$], a, b, c and d are the parameters. The third-order polynomial term in the above equation considers the baseline offset in the measured extinction occurring due to the unspecified optical losses mentioned earlier. This method was previously implemented in several IBBCEAS studies dealing with absolute concentration retrieval (J. Chen, 2011; Dixneuf, Ruth, Vaughan, Varma, & Orphal, 2009; Gherman et al., 2008; Varma et al., 2009; D. S. Venables et al., 2006).

The unknown quantities in equation 16, viz., *a*, *b*, *c*, *d* and number density of all the gases (*n*) were retrieved using a linear algebraic technique known as singular-value decomposition (SVD) method (Press, 2007). With 8 unknown parameters and over 100 equations in the wavelength range of 1100-1250 nm for each measurement, the process is an overdetermined problem. A MATLAB routine for SVD based on linear least squares approach was developed to fit equation 16 to the measured extinction coefficient. The SVD procedure is discussed below.

Using equation 16, a $n \times p$ matrix *A* could be formed as follows, where *n* denotes the number of λ and *p* is the number of fit parameters ($p = 8$ in this case).

$$A = \begin{bmatrix} 1 & \lambda_1 & \lambda_1^2 & \lambda_1^3 & \sigma_{CH_4}(\lambda_1) & \sigma_{C_2H_6}(\lambda_1) & \sigma_{C_3H_8}(\lambda_1) & \sigma_{C_4H_{10}}(\lambda_1) \\ 1 & \lambda_2 & \lambda_2^2 & \lambda_2^3 & \sigma_{CH_4}(\lambda_2) & \sigma_{C_2H_6}(\lambda_2) & \sigma_{C_3H_8}(\lambda_2) & \sigma_{C_4H_{10}}(\lambda_2) \\ . & . & . & . & . & . & . & . \\ . & . & . & . & . & . & . & . \\ 1 & \lambda_n & \lambda_n^2 & \lambda_n^3 & \sigma_{CH_4}(\lambda_n) & \sigma_{C_2H_6}(\lambda_n) & \sigma_{C_3H_8}(\lambda_n) & \sigma_{C_4H_{10}}(\lambda_n) \end{bmatrix}, \quad (17)$$

The rectangular matrix A serves as the input for the SVD function in MATLAB which calculates a set of three matrices, $U_{n \times n}$, $S_{n \times p}$, and $V_{p \times p}$ such that $A = U\,S\,V^T$. Columns of U and V are left- and right-singular vectors respectively while S is a diagonal matrix of singular values. Further, a diagonal matrix W was formed which contains the reciprocal of the diagonal elements of S. Using these, the unknown coefficients' matrix ($C_{p \times 1}$) were retrieved as,

$$C = V \times W \times (U^T \times \alpha), \tag{18}$$

where × denotes matrix multiplication, and α is a column vector of length n. The fit uncertainties in the retrieved coefficients were calculated using the sum of square of residuals and covariance matrix. Covariance matrix was determined by,

$$CovMat = V \times W^2 \times V^T, \tag{19}$$

and the uncertainties were calculated as,

$$u_C = \sqrt{\left(\frac{\sum\left((A \times C) - \alpha\right)^2}{n - p}\right) \times diag(CovMat)}, \tag{20}$$

The choice of SVD analysis over the nonlinear Levenberg-Marquardt routine (Tao Wu, Coeur-Tourneur, et al., 2014) was mainly due to the faster real-time analysis in SVD method. Previous studies (Varma et al., 2009; Yi et al., 2016) have also reported similar results employing both the

techniques. Moreover, fittings in the iterative methods are influenced by choice of initial parameters. But in SVD technique, due to the absence of start parameter selection, the fit outcomes do not experience such an impact. Hence, SVD seemed to be an efficient option. The SVD routine was incorporated inside the NIR-IBBCEAS LabVIEW program discussed in section 4.3.

5.2.2 Error Analysis

Experimental measurements are prone to uncertainties due to several factors including instrument precision, variation in experimental parameters and mathematical approximations. All these errors tend to propagate throughout the analysis. The estimation of measurement uncertainty in the retrieved number densities of gases from equation 16 was carried out using the standard propagation of error approach (Ku, 1966).

The uncertainties in the retrieved concentrations mainly arise through the uncertainty in measured extinction coefficient and absorption cross-sections. The extinction coefficient of the sample is obtained using equation 15. Uncertainty in its measurement, which was common to all spectra, was calculated using (J. Chen, 2011; Varma et al., 2009),

$$\Delta\alpha^2 = \left|\frac{\partial\alpha}{\partial(1-R)}\right|^2 \Delta(1-\mathrm{R})^2 + \left|\frac{\partial\alpha}{\partial L}\right|^2 \Delta\mathrm{L}^2 + \left|\frac{\partial\alpha}{\partial I_0}\right|^2 \Delta {I_0}^2 , \qquad (21)$$

where $\Delta\alpha$, $\Delta(1\text{-}R)$, ΔL and ΔI_0 denote the uncertainties in extinction coefficient, mirror reflectivity, cavity length and light intensity respectively. Using fractional uncertainties, a simpler and inherent form of equation 21 would be,

$$\left(\frac{\Delta\alpha}{\alpha}\right)^2 = \left(\frac{\Delta(1-\mathrm{R})}{1-R}\right)^2 + \left(\frac{\Delta \mathrm{L}}{L}\right)^2 + \left(\frac{\Delta I_0}{I_0}\right)^2, \quad (22)$$

The mean percentage error of L and I_0 were found to be 0.8% and 4%. Since the cavity length was measured using a ruler, the maximum error occurring in its measurement was estimated to be 0.5 cm (about 0.8%). The error in I_0 was found from the mean deviation of intensities in the wavelength range of 1100-1250 nm from I_0 spectra recorded for 10 minutes. The uncertainty of (*1-R*) is limited by the uncertainty associated with the convolution of HITRAN cross-section values of methane and carbon dioxide to the instrument resolution along with the error in L, I_0 and number density calculations. Uncertainty in the convolution process was estimated to be about 2% while the error in determining number concentration, which was mainly attributed to the pressure inside the cavity volume, was estimated to be 6%. Convolution error was estimated from the mean deviation of convolved spectra at all the four laser peaks discussed in section 3.2 while the uncertainty in pressure was assigned to be 1 psi. Then, using a procedure similar to equations 21 and 22, the uncertainty in determining (*1-R*) was estimated to be 7.5%. Hence, the net uncertainty in extinction measurement was calculated as 8.5%.

The uncertainty in the cross-section values of butane, ethane, and propane was mainly due to the error in measured extinction and number concentration. Using their fractional uncertainties (discussed above), the uncertainty of reference absorption cross-section values was estimated to be 11% (equation 23).

$$\left(\frac{\Delta\sigma}{\sigma}\right)^2 = \left(\frac{\Delta\alpha}{\alpha}\right)^2 + \left(\frac{\Delta n}{n}\right)^2, \quad (23)$$

Finally, the expected uncertainties in the retrieved gas concentration of each species were evaluated using,

$$\Delta {n_{i,fit}}^2 = \left|\frac{\partial n_i}{\partial \alpha}\right|^2 \Delta\alpha^2 + \left|\frac{\partial n_i}{\partial \sigma_i}\right|^2 \Delta {\sigma_i}^2, \quad (24)$$

which could also be written as,

$$\left(\frac{\Delta n_{i,fit}}{n_{i,fit}}\right)^2 = \left(\frac{\Delta\alpha}{\alpha}\right)^2 + \left(\frac{\Delta\sigma}{\sigma}\right)^2, \quad (25)$$

Here, *i* denotes the species. The net uncertainty in methane concentration was therefore about 10% while that of butane, ethane, and propane was approximately 14% each. These numbers denote the maximum error that could propagate along the calculations due to the uncertainty in measurement variables apart from the fitting error of linear least square SVD approach.

5.3 Instrument Testing

Since methane forms the major component of natural gas, detection of methane dominates the natural gas leak detection process. Hence, a 995.1 ppm methane gas sample was used to demonstrate the instrument's leak detection capability. To showcase its ability to determine the hydrocarbon composition of a natural gas mixture, the instrument was also tested on a mixture

containing 2.002% methane, 1.506% ethane, 0.9965% propane, 1.006% butane and balance nitrogen. All the gases were introduced at 1 atm pressure and ambient temperature (23ºC). The experiment details and results are presented in this section.

5.3.1 995.1 ppm Methane sample

In order to determine the accuracy and sensitivity of the NIR-IBBCEAS instrument in detecting natural gas leaks, the instrument was tested on a 995.1 ppm methane gas sample in balance nitrogen from Praxair, Inc., Canada. The process was controlled and monitored through the NIR-IBBCEAS software where the dark (I_{dark}) and I_0 spectra were measured before introducing

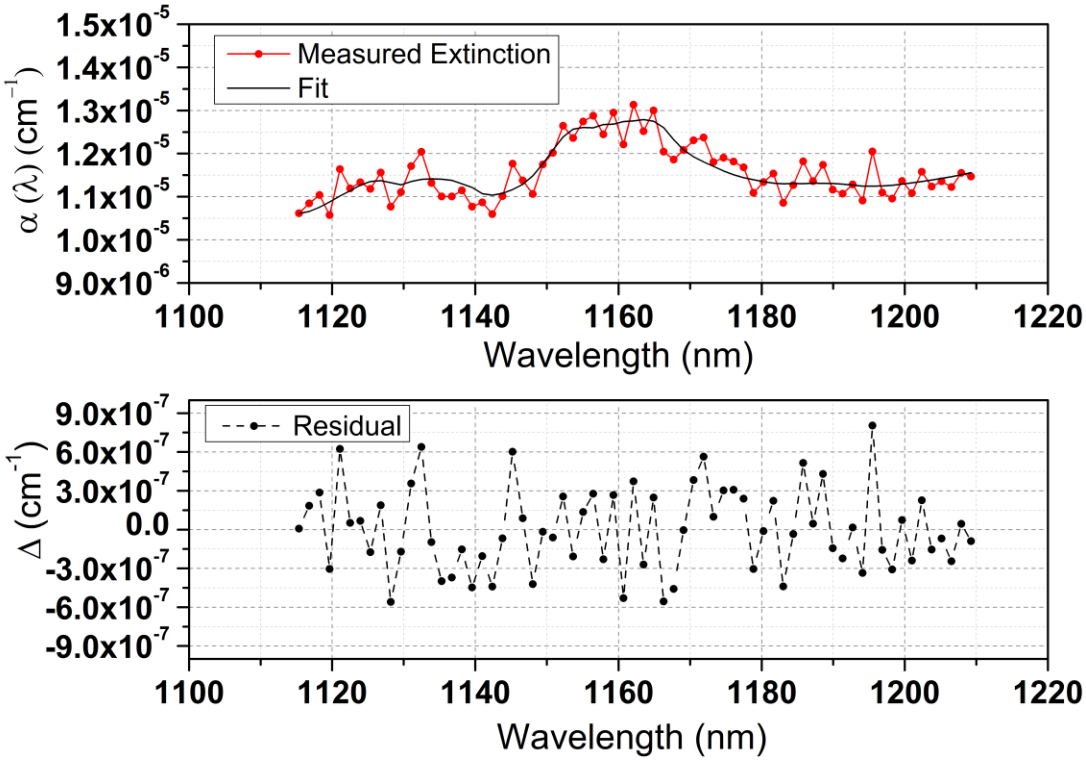

Figure 23: Upper panel: Extinction coefficient of 995.1 ppm methane measured using the NIR-IBBCEAS instrument (dotted-line spectrum). The solid line denotes nonlinear least square generated according to equation 16. Lower panel: Absolute residuals of the fit.

methane. The extinction measurement of the gas was measured using a spectrometer gain of 64 and by averaging 30 spectra at an integration time of 1 second.

Figure 23 shows the measured average extinction of 995.1 ppm methane in balance nitrogen using the NIR-IBBCEAS instrument. The concentration retrieved from the fit was 1045.6 ± 104.7 ppm. The stated error (104.7 ppm) in the retrieved concentration denotes the quality of fit rather than the measurement uncertainty.

5.3.1.1 Signal to Noise Ratio

Using a single-point consideration, the signal to noise ratio of the measurement could be estimated by defining it as the ratio of methane absorption maximum and the noise in the measurement (D. S. Venables et al., 2006). From Figure 23, the absorption maximum of methane is approximately, $\alpha_{max} = 1.30 \times 10^{-5}$ cm^{-1}. The noise in the measurement was defined as the standard deviation of the fit residual. The standard deviation (1σ) of the residual depicted in Figure 23 was approximately 3.19×10^{-7} cm^{-1}. Then, the signal-to-noise ratio was calculated as,

$$\mathrm{SNR} = \frac{\alpha_{\max}}{1\sigma} \approx 41, \tag{26}$$

5.3.1.2 Detection limit

There are different methods to quantify detection limit for monitoring methods (EPA, 2016). One way to determine the method detection limit (MDL) is by multiplying the Student-t value for a 95% or 99% confidence interval with the standard deviation (CFR, 1984; EPA, 2016). The

limit of detection (LOD) could also be defined as 10% below the smallest concentration within a standard curve or 3 times the SNR. Two of the popular methods of LOD estimation is to define LOD as 3 times the standard deviation of results from a low concentration sample or as 3 times the response of the method noise (EPA, 2016). Considering the detection limit to be three times the noise level of measurement (3σ), we could estimate the detection limit of methane, butane, ethane, and propane by comparing their absorption cross-section maximum with 3σ (Y. Chen et al., 2016; Gherman et al., 2008; D. S. Venables et al., 2006). The maximum absorption cross-section of methane, butane, ethane and propane are 8.48×10^{-23} (1163.5 nm), 2.76×10^{-22} (1185.81 nm), 2.23×10^{-22} (1181.64 nm) and 2.26×10^{-22} (1189.97 nm) cm^2 $molecule^{-1}$ respectively. The 3σ of fit residual was approximately 9.57×10^{-7} cm^{-1}. Then, the corresponding detection limits were approximately 460 ppm, 141 ppm, 175 ppm and 173 ppm for methane, butane, ethane, and propane respectively considering the ambient conditions as 1 atm and 296 K. The reported Lower Explosive Limits (LEL) for methane, butane, ethane and propane at ambient conditions are 5%, 1.8%, 3% and 2.1% by volume respectively (Gas, 2013; Liao, Cheng, Jiang, & Gao, 2005). Hence, the obtained detection limits are well less than 1% of their LEL (Methane-0.92%LEL, butane-0.78%LEL, ethane-0.58%LEL and propane-0.82%LEL).

It should also be noted that the reported detection limits are based on the traditional single-point technique, which considered only the absorption maximum of each gas. However, if we consider the entire absorption spectrum, the detection limits would be lower. Moreover, the discussed limits are for the given experimental conditions (average of 30 scans with an integration time of 1 second). Longer integration time along with a longer optical cavity (current length is 60 cm) may result in better detection sensitivities.

5.3.2 Hydrocarbon Mixture

As described earlier, another useful application of this instrument is to study the quality of gas mixture. In principle, by looking at the IBBCEAS absorption of natural gas over the wavelength range of 1100-1250 nm, the instrument could retrieve the composition of methane, butane, ethane, and propane in the mixture. To test this, a mixture containing 2.002% methane, 1.506% ethane, 0.9965% propane, 1.006% butane and balance nitrogen from Praxair, Inc., Canada was employed. The extinction measurement of the mixture was conducted after the measurements of I_{dark} and I_0 (nitrogen) like before. The spectrometer parameters were also retained from the methane measurement (Gain-64 and Averaging-30).

Figure 24 depicts the measured NIR-IBBCEAS extinction of the mixture.

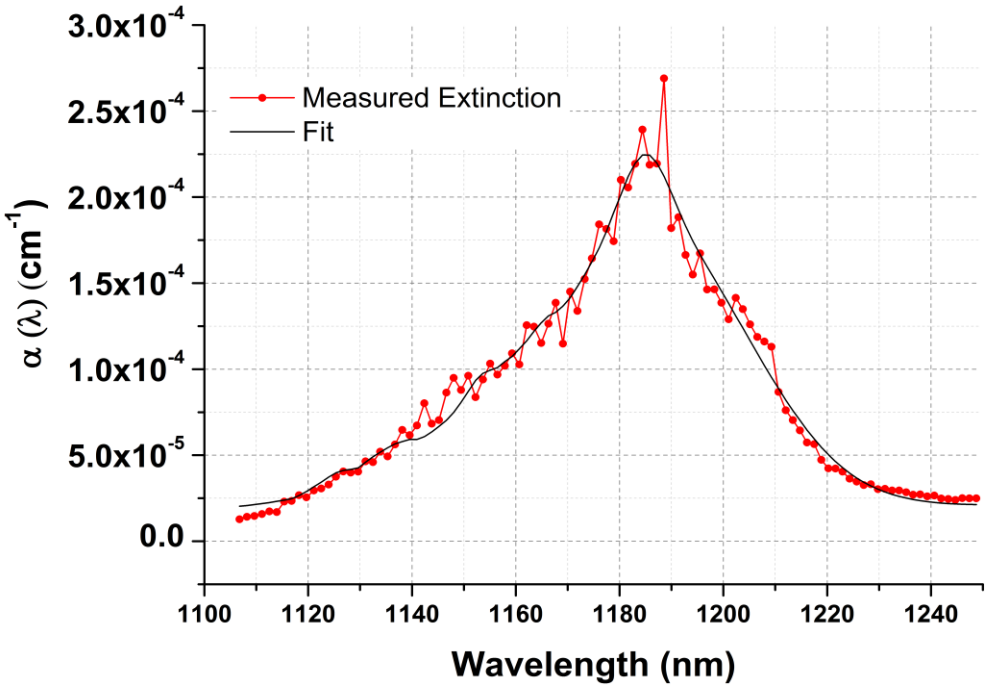

Figure 24: Measured extinction coefficient of the mixture from the NIR-IBBCEAS instrument (dotted-line spectrum). The solid line denotes least square fit generated according to equation 16.

It should be noted that the absorption cross-section of propane overlaps almost completely with that of butane (Figure 25). Hence, it was difficult to accurately differentiate the contributions of propane and butane towards the total extinction due to the overlapping spectral features. Therefore, their contribution is reported as the combined concentration of propane and butane. However, an extension of wavelength range to include the separated absorption features would enable differentiation of propane and butane and their separate quantification.

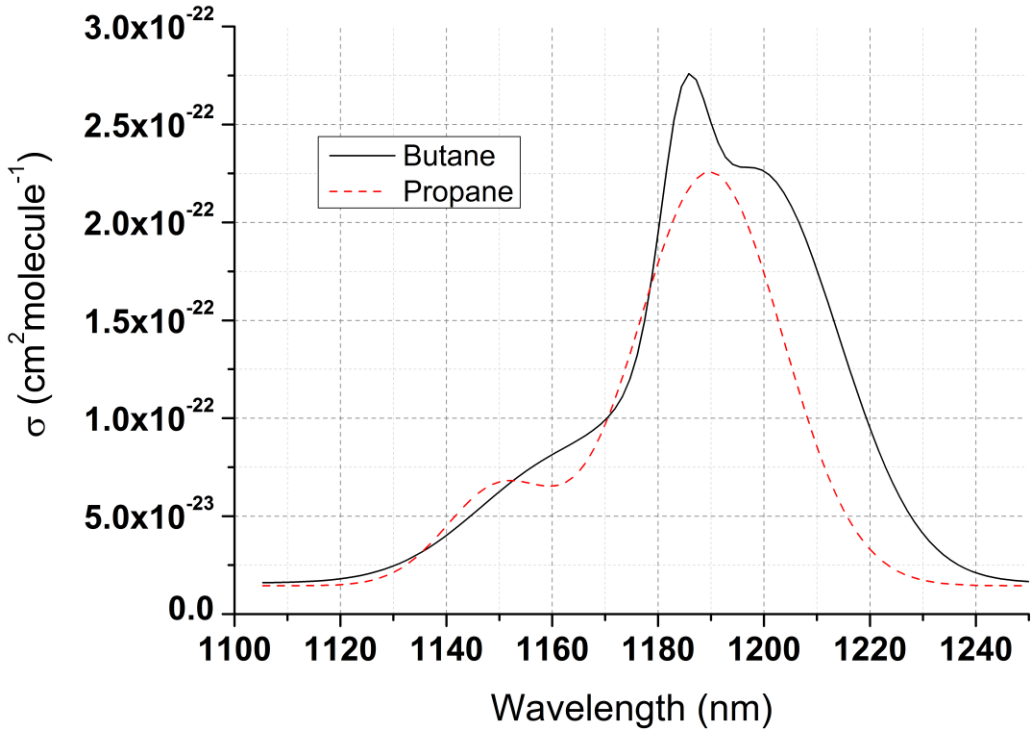

Figure 25: Overlapping absorption cross-section of propane and butane.

The spectral fitting on the measured extinction (Figure 24) estimated the concentrations of methane, ethane, and propane + butane combined to be 1.86 ± 0.19%, 1.51 ± 0.14% and 2.05 ± 0.23% respectively. As mentioned earlier, the stated error is just an indication of the quality of the fitting rather than the measurement uncertainty. The retrieved concentrations were well within the predicted maximum measurement uncertainties in the concentration retrieval for each component (section 5.2.2).

Chapter 6: Conclusion

6.1 Summary of Findings

The principle of near-infrared incoherent broadband cavity enhanced absorption spectroscopy (NIR-IBBCEAS) was used to develop and demonstrate a low-cost, highly sensitive gas leak detector for simultaneous leak detection of methane (natural gas), ethane, propane, and butane. As per the author's best knowledge, this is the first such attempt using the technique of NIR-IBBCEAS. The choice of NIR region helped in reducing the water vapor interferences and the instrumentation cost. It also helped in the multiple species detections due to the weaker nature of hydrocarbon absorption in this region.

A NIR-IBBCEAS system using a supercontinuum laser was developed at the Environmental Optics Laboratory (EOL) at Michigan Technological University (MTU), Houghton, USA, for the initial laboratory testing of the method's feasibility. Based on the observed appreciable absorbance of methane and butane even at low concentration and minimum laser power, it was inferred that the application of NIR IBBCEAS in the 1100 to 1250 nm wavelength range using a tungsten-halogen light source can efficiently detect all the four hydrocarbons under consideration (methane, butane, ethane, and propane).

A similar NIR-IBBCEAS system was installed at the Applied Optics & Instrumentation Lab, Department of Physics, National Institute of Technology Calicut (NITC), India, to measure the absorption cross-section values of butane, ethane, and propane in the instrument resolution since these were not available in the literature. The xenon short arc lamp-based system used the NIRez spectrometer whose wavelength scale was calibrated, and the resolution was estimated to be 8.71 nm. With a moderate mirror reflectivity (0.999), the absorption cross-sections of butane, ethane,

and propane were estimated in the wavelength range of 1100-1250 nm. The maximum absorption cross-section values of butane, ethane, and propane were reported as 2.76×10^{-22} (1185.81 nm), 2.23×10^{-22} (1181.64 nm) and 2.26×10^{-22} (1189.97 nm) cm^2 $molecule^{-1}$ respectively.

After the preliminary experiments, the NIR-IBBCEAS gas leak detector, using a tungsten-halogen source, was developed on an aluminum extrusion framework. The instrument was tested on a 995.1 ppm methane and a hydrocarbon mixture containing 2.002% methane, 1.506% ethane, 0.9965% propane, 1.006% butane with balance nitrogen. The retrieved concentrations were in excellent agreement with the data provided by the gas suppliers, with the error being within the expected uncertainties. The detection limits of the instrument with the current experimental parameters were estimated to be approximately 460 ppm, 141 ppm, 175 ppm and 173 ppm for methane, butane, ethane, and propane respectively. These values are well below the LEL limits of gases (<1% of LEL). In short, a cost-effective, sensitive and real-time natural gas leakage detector can be developed using the well-established IBBCEAS technique.

6.2 Key Highlights

The developed NIR-IBBCEAS gas leak detector has a number of possible applications and benefits. It could be used as a detector for individual leak detection of methane, butane, ethane, propane or natural gas leaks. It could also be used for detecting the leak of hydrocarbon mixtures containing any combinations of the above gases. It could be installed in confined areas, indoors and closed industrial facilities to detect gas leaks. It could also be used to analyze leak in small sections of gas pipeline and joints. Further miniaturization of the design could help in deploying it as a household natural gas detector. The instrument also serves the purpose of testing the

quality of a natural gas mixture quite effectively owing to the SVD routine retrieving the composition of the major hydrocarbon constituents of the mixture. However, it should be noted that, currently, due to the complete overlap of propane spectral feature with that of butane in the selected wavelength range, the contribution of butane and propane were reported together. This drawback could be eliminated by extending the wavelength range.

To detect a natural gas leak, since the instrument performs simultaneous monitoring of the major hydrocarbons of the natural gas mixture over a broad range of wavelengths, they are less prone to false alarms compared to other laser-based techniques, which only quantify a single gas at a time. While most of the current hand-held and vehicle-mounted FID and IR detectors are slow and labor intensive, the developed NIR-IBBCEAS technology can be fast and efficient if installed in an open path configuration with a long optical path. Some of the newer laser-based techniques, like the Boreal laser leak detection, achieve a detection limit of around 0.2 ppm with a smaller dynamic range (0-100 ppm) through airborne measurements of the methane plume emitted due to the gas leaks. Even though the detection limit of this prototype is quite high compared to such techniques, it provides a larger dynamic range to work with (for example, the methane detection limit of this instrument is 460 ppm while the reflectivity calibration was performed using approximately 5% by volume methane). Moreover, to differentiate the methane leaks from ambient methane concentrations, a higher detection limit may be more useful. If carefully designed, the developed instrument could be improved to achieve sensitivities capable of detecting small leaks in ground-based deployment at a much lower cost (for instance, several past IBBCEAS instrumentations have achieved detection limits in ppt and ppb levels for atmosphere trace species like NO_3, NO_2 and HONO (Gherman et al., 2008; D. S. Venables et al., 2006)). This is briefed in the later section. It also suites the purpose of a cheaper continuous

long-time monitoring of gas leak over a region rather than the occasional costlier flight measurements.

6.3 Assumptions and Limitations

It should be noted that the results presented in the study contained certain assumptions. Since the water vapor absorption is negligible in this region of wavelength (1100 - 1250 nm), the interference due to water vapor is ignored in this study. The unknown losses in this wavelength range are also assumed to be due to unstructured loss processes like intensity fluctuations and the 3rd order polynomial term in the fitting routine account for them. Moreover, the detection limits were statistically estimated assuming the detection limits to be 3 times the noise in the measurements rather than systematically testing it using different concentrations of each gases. A possible limitation in its long-term monitoring applications would be the need to measure I_0 at regular intervals due to the long-term intensity drift of the light source. One way to do this would be by manually closing the cavity volume at regular intervals and flushing the space with nitrogen gas. However, a more convenient option would be to install a small separate nitrogen gas-filled cell inside the instrument and to deflect a small portion of light into this. This would help in auto-tracking the intensity drift.

6.4 Future Work

Compared to the contemporary laser-based methods, the developed instrument has a higher detection limit and lower SNR. Due to the overlapping features, it was also found that butane and propane could not be differentiated accurately. Hence, one of the possible directions of improvement is in the sensitivity of detection. Even though the detection limit achieved using the

current set-up is less than 1% of the LEL limits of gases, the sensitivity can be further enhanced through better instrumentation. In IBBCEAS technique, increasing the cavity length can increase the detection sensitivity of the instrument. To implement it in the current system, a more intense light source is also required to obtain the sufficient cavity signal intensity at longer cavity length. This can be achieved by replacing the current 75 W tungsten-halogen bulb with a higher wattage bulb. The sensitivity of the current instrument is also limited by the high noise levels of NIRez spectrometer. Hence, the signal to noise ratio can be improved by using a lower-noise spectrometer and thereby achieving better sensitivity. The signal to noise ratio can also be improved by utilizing a longer integration time. Another way to achieve better detection limit is by monitoring absorption at multiple absorption feature regions. As shown by Rohwedder et al. (Rohwedder et al., 2014), the hydrocarbons under current study have another absorption feature between 1260 nm and 1550 nm. Hence, increased accuracy and enhanced detection limits could also be achieved by utilizing dielectric mirrors with high reflectivity in both these spectral regions (1100-1250 nm and 1260-1550 nm). This would also help in differentiating butane and propane with better accuracy.

A detailed analysis on the repeatability of results would be useful to further strengthen the application prospects of the instrument. Currently, the tests were performed using a single mixture of methane, ethane, propane, and butane. It is important to study the quantification errors for different combinations of hydrocarbons such as methane + ethane, or ethane + butane, or ethane + butane + propane etc. This would provide a better understanding of selectivity of the SVD routine.

Another possible future work would be to study the effects of change in proportions of different components in the mixture. Currently, the results presented in the thesis used a proportion of

approximately 2:1.5:1:1 for methane:ethane:propane:butane and the errors in retrieval were within 10%. It would be interesting to study the consistency in the retrieval errors by varying the proportions. One could also determine a threshold proportion (limit of recognition), if it exists, below which the error in differentiating the components would be large.

References

Aalto, A., Genty, G., Laurila, T., & Toivonen, J. (2015). Incoherent broadband cavity enhanced absorption spectroscopy using supercontinuum and superluminescent diode sources. *Optics express, 23*(19), 25225-25234.

Adams, T. J. (2016). *Atmospheric Measurements of Biogenic and Anthropogenic Emissions by Broadband Cavity Enhanced Absorption Spectroscopy.* Department of Chemistry.

Aksoy, M. (1989). Hematotoxicity and carcinogenicity of benzene. *Environmental Health Perspectives, 82*, 193.

Allen, D. T., Torres, V. M., Thomas, J., Sullivan, D. W., Harrison, M., Hendler, A., . . . Hill, A. D. (2013). Measurements of methane emissions at natural gas production sites in the United States. *Proceedings of the National Academy of Sciences, 110*(44), 17768-17773.

Althouse, M. L., & Chang, C.-I. (1995). *Chemical vapor detection and mapping with a multispectral forward-looking infrared (FLIR).* Paper presented at the Optical Instrumentation for Gas Emissions Monitoring and Atmospheric Measurements.

Amirante, R., Distaso, E., Di Iorio, S., Sementa, P., Tamburrano, P., Vaglieco, B., & Reitz, R. (2017). Effects of natural gas composition on performance and regulated, greenhouse gas and particulate emissions in spark-ignition engines. *Energy Conversion and Management, 143*, 338-347.

Axson, J., Washenfelder, R., Kahan, T., Young, C., Vaida, V., & Brown, S. (2011). Absolute ozone absorption cross section in the Huggins Chappuis minimum (350–470 nm) at 296 K. *Atmospheric Chemistry and Physics, 11*(22), 11581-11590.

Ball, S. M., & Jones, R. L. (2003). Broad-band cavity ring-down spectroscopy. *Chemical reviews, 103*(12), 5239-5262.

Baughcum, S. L. (1996). Subsonic aircraft emission inventories. *Atmospheric effects of aviation: First report of the subsonic assessment project*, 15-29.

Bennett, C. L., Carter, M. R., & Fields, D. J. (1995). *Hyperspectral imaging in the infrared using LIFTIRS.* Paper presented at the Infrared Technology XXI.

Berden, G., & Engeln, R. (2009). *Cavity ring-down spectroscopy: techniques and applications*: John Wiley & Sons.

Bernhardt, B., Ozawa, A., Jacquet, P., Jacquey, M., Kobayashi, Y., Udem, T., . . . Picqué, N. (2010). Cavity-enhanced dual-comb spectroscopy. *Nature Photonics, 4*(1), 55.

Blokker, P. (1972). A literature survey on some health aspects of lead emissions from gasoline engines. *Atmospheric Environment (1967), 6*(1), 1-18.

Bose, J., & Olson, M. (1993). TAPS's leak detection seeks greater precision. *Oil and Gas Journal;(United States), 91*(14).

Burdett, R. (2005). Signals in the Presence of Noise. *Handbook of Measuring System Design*.

Carlson, B. N. (1993). *Selection and use of pipeline leak detection methods for liability management into the 21st century.* Paper presented at the Pipeline Infrastructure II.

CFR. (1984). Appendix B: definition and procedure for the determination of the method detection limit (Vol. 136).

Chandran, S., & Varma, R. (2016). Near infrared cavity enhanced absorption spectra of atmospherically relevant ether-1, 4-Dioxane. *Spectrochimica Acta Part A: Molecular and Biomolecular Spectroscopy, 153*, 704-708. doi:http://dx.doi.org/10.1016/j.saa.2015.09.030

Chang, M.-C. O., Chow, J. C., Watson, J. G., Hopke, P. K., Yi, S.-M., & England, G. C. (2004). Measurement of ultrafine particle size distributions from coal-, oil-, and gas-fired stationary combustion sources. *Journal of the Air & Waste Management Association, 54*(12), 1494-1505.

Chen, J. (2011). Broadband optical cavity absorption spectroscopy in the near-ultraviolet: applications in atmospheric chemistry.

Chen, Y., Yang, C., Zhao, W., Fang, B., Xu, X., Gai, Y., . . . Zhang, W. (2016). Ultra-sensitive measurement of peroxy radicals by chemical amplification broadband cavity-enhanced spectroscopy. *Analyst, 141*(20), 5870-5878.

Davies, P. (2001). The new challenge of natural gas. *OPEC and the global energy balance: towards a sustainable future, Vienna, 28*.

Dedikov, J., Akopova, G., Gladkaja, N., Piotrovskij, A., Markellov, V., Salichov, S., . . . Lelieveld, J. (1999). Estimating methane releases from natural gas production and transmission in Russia. *Atmospheric Environment, 33*(20), 3291-3299.

Demirbas, A. (2006). The importance of natural gas as a world fuel. *Energy Sources, Part B, 1*(4), 413-420.

Demtröder, W. (1971). *Laser spectroscopy* (Vol. 17): Springer.

Denzer, W., Hamilton, M., Hancock, G., Islam, M., Langley, C., Peverall, R., & Ritchie, G. (2009). Near-infrared broad-band cavity enhanced absorption spectroscopy using a superluminescent light emitting diode. *Analyst, 134*(11), 2220-2223.

Dixneuf, S., Ruth, A., Vaughan, S., Varma, R., & Orphal, J. (2009). The time dependence of molecular iodine emission from Laminaria digitata. *Atmospheric Chemistry and Physics, 9*(3), 823-829.

Engeln, R., & Meijer, G. (1996). A Fourier transform cavity ring down spectrometer. *Review of scientific instruments, 67*(8), 2708-2713.

EPA. (2016). *Detection Limit/Quantitation Limit Summary Table*. www.epa.gov Retrieved from https://www.epa.gov/sites/production/files/2016-11/documents/mdlmql-toolbox-_final_nov2016_0.pdf.

Fiedler, S. E., Hese, A., & Ruth, A. A. (2003). Incoherent broad-band cavity-enhanced absorption spectroscopy. *Chemical Physics Letters, 371*(3–4), 284-294. doi:http://dx.doi.org/10.1016/S0009-2614(03)00263-X

Finkelman, R. B., Belkin, H. E., & Zheng, B. (1999). Health impacts of domestic coal use in China. *Proceedings of the National Academy of Sciences, 96*(7), 3427-3431.

Finlayson-Pitts, B. J., & Pitts Jr, J. N. (1986). Atmospheric chemistry. Fundamentals and experimental techniques.

Finlayson-Pitts, B. J., & Pitts Jr, J. N. (1999). *Chemistry of the upper and lower atmosphere: theory, experiments, and applications*: Academic press.

Foltynowicz, A., Schmidt, F. M., Ma, W., & Axner, O. (2008). Noise-immune cavity-enhanced optical heterodyne molecular spectroscopy: Current status and future potential. *Applied Physics B, 92*(3), 313.

Gaffney, J. S., & Marley, N. A. (2009). The impacts of combustion emissions on air quality and climate–From coal to biofuels and beyond. *Atmospheric Environment, 43*(1), 23-36.

Gas, L. (2013). Lower and upper explosive limits for flammable gases and vapors (LEL/UEL). *Matheson gas products*, 22.

Gherman, T., Venables, D. S., Vaughan, S., Orphal, J., & Ruth, A. A. (2008). Incoherent Broadband Cavity-Enhanced Absorption Spectroscopy in the near-Ultraviolet: Application to HONO and NO2. *Environmental Science & Technology, 42* (3), 890-895. doi:10.1021/es0716913

Goldemberg, J. (2006). The promise of clean energy. *Energy policy, 34*(15), 2185-2190.

Gopalsami, N., & Raptis, A. C. (2001). Millimeter-wave radar sensing of airborne chemicals. *IEEE Transactions on Microwave Theory and Techniques, 49*(4), 646-653.

Gorse, R. A., Benson, J. D., Burns, V. R., Hochhauser, A. M., Koehl, W. J., Painter, L. J., . . . Rippon, B. H. (1991). *Toxic air pollutant vehicle exhaust emissions with reformulated gasolines* (0148-7191). Retrieved from

Griebenow, G., & Mears, M. (1989). Leak detection implementation: modeling and tuning methods. *Journal of Energy Resources Technology, 111*(2), 66-71.

Hansen, J., Sato, M., Ruedy, R., Lacis, A., & Oinas, V. (2000). Global warming in the twenty-first century: An alternative scenario. *Proceedings of the National Academy of Sciences, 97*(18), 9875-9880.

Harrison, R. M. (2004). Key pollutants—airborne particles. *Science of the total Environment, 334*, 3-8.

Herriott, D. R., & Schulte, H. J. (1965). Folded optical delay lines. *Applied Optics, 4*(8), 883-889.

Hodgkinson, J., & Tatam, R. P. (2012). Optical gas sensing: a review. *Measurement Science and Technology, 24*(1), 012004.

Hoeks, J. (1972). *Effect of leaking natural gas on soil and vegetation in urban areas*: Pudoc.

Hough, J. E. (1988). Leak testing of pipelines uses pressure and acoustic velocity. *Oil Gas J.;(United States), 86*(47).

Howarth, R., Shindell, D., Santoro, R., Ingraffea, A., Phillips, N., & Townsend-Small, A. (2012). Methane emissions from natural gas systems. Background paper prepared for the National Climate Assessment, Reference# 2011-003, Office of Science & Technology Policy Assessment, Washington, DC.

Husar, R. B. (1986). Emissions of sulfur dioxide and nitrogen oxides and trends for eastern North America. *Acid Deposition Long-Term Trends. National Research Council. National Academy Press, Washington, DC*.

Ikuta, K., Yoshikane, N., Vasa, N., Oki, Y., Maeda, M., Uchiumi, M., . . . Kawada, N. (1999). Differential absorption lidar at 1.67 μm for remote sensing of methane leakage. *Japanese journal of applied physics, 38*(1R), 110.

Iseki, T., Tai, H., & Kimura, K. (2000). A portable remote methane sensor using a tunable diode laser. *Measurement Science and Technology, 11*(6), 594.

Jackson, R. B., Down, A., Phillips, N. G., Ackley, R. C., Cook, C. W., Plata, D. L., & Zhao, K. (2014). Natural gas pipeline leaks across Washington, DC. *Environmental Science & Technology, 48*(3), 2051-2058.

Jackson, R. B., Vengosh, A., Darrah, T. H., Warner, N. R., Down, A., Poreda, R. J., . . . Karr, J. D. (2013). Increased stray gas abundance in a subset of drinking water wells near Marcellus shale gas extraction. *Proceedings of the National Academy of Sciences, 110*(28), 11250-11255.

Karion, A., Sweeney, C., Pétron, G., Frost, G., Michael Hardesty, R., Kofler, J., . . . Banta, R. (2013). Methane emissions estimate from airborne measurements over a western United States natural gas field. *Geophysical Research Letters, 40*(16), 4393-4397.

Karpf, A., & Rao, G. N. (2015). Real-time trace gas sensor using a multimode diode laser and multiple-line integrated cavity enhanced absorption spectroscopy. *Applied Optics, 54*(19), 6085-6092.

Kato, K., Igarashi, K., Masuda, M., Otsubo, K., Yasuda, A., Takeda, K., & Sato, T. (1999). *Development of engine for natural gas vehicle* (0148-7191). Retrieved from

Kebabian, P. L., & Freedman, A. (2007). System and method for trace species detection using cavity attenuated phase shift spectroscopy with an incoherent light source: Google Patents.

King, S. R. (1992). *The impact of natural gas composition on fuel metering and engine operational characteristics* (0148-7191). Retrieved from

Kirchstetter, W., Miguel, H., & Harley, A. (1998). *On-road comparison of exhaust emissions from gasoline and diesel engines.* Paper presented at the Proceedings of the Eighth CRC On-road Vehicle Emissions Workshop, April.

Klein, W. (1993). Acoustic leak detection. *American Society of Mechanical Engineers, Petroleum Division, 55*, 57-61.

Kowalewicz, A. (1984). Combustion systems of high-speed piston IC engines.

Ku, H. H. (1966). Notes on the use of propagation of error formulas. *Journal of Research of the National Bureau of Standards, 70*(4).

Kulp, T. J., Kennedy, R. B., DeLong, M. L., Garvis, D. G., & Stahovec, J. (1993). *Development and testing of a backscatter absorption gas imaging (BAGI) system capable of imaging at a range of 300 m.* Paper presented at the Applied Laser Radar Technology.

Kulp, T. J., Powers, P. E., & Kennedy, R. B. (1997). *Remote imaging of controlled gas releases using active and passive infrared imaging systems.* Paper presented at the Infrared Technology and Applications XXIII.

Lechtenböhmer, S., Dienst, C., Fischedick, M., Hanke, T., Fernandez, R., Robinson, D., . . . Gillis, B. (2007). Tapping the leakages: Methane losses, mitigation options and policy issues for Russian long distance gas transmission pipelines. *International journal of greenhouse gas control, 1*(4), 387-395.

Lehmann, K. K., & Romanini, D. (1996). The superposition principle and cavity ring-down spectroscopy. *The Journal of chemical physics, 105*(23), 10263-10277.

Liao, S., Cheng, Q., Jiang, D., & Gao, J. (2005). Experimental study of flammability limits of natural gas–air mixture. *Journal of hazardous materials, 119*(1-3), 81-84.

Liou, J. C., & Tian, J. (1995). Leak detection—transient flow simulation approaches. *Journal of Energy Resources Technology, 117*(3), 243-248.

Liss, W., Thrasher, W., Steinmetz, G., Chowdiah, P., & Attari, A. (1992). *Variability of natural gas composition in select major metropolitan areas of the united states. final report, august 1990-february 1992*. Retrieved from

Lloyd, A. C., & Cackette, T. A. (2001). Diesel engines: environmental impact and control. *Journal of the Air & Waste Management Association, 51*(6), 809-847.

Ly, H. (2002). *Effects of natural gas composition variations on the operation, performance and exhaust emissions of natural gas-powered vehicles.* Paper presented at the NGV 2002 Conference Paper-Effects of Gas Composition-Aug.

McClure, W. F. (1994). Near-infrared spectroscopy. The giant is running strong. *Analytical chemistry, 66*(1), 43A-53A.

Medina, D. S. (2011). *Instrument Development and Measurements of the Atmospheric Pollutants Sulfur Dioxide, Nitrate Radical, and Nitrous Acid by Cavity Ring-down Spectroscopy and Cavity Enhanced Absorption Spectroscopy*. UC Riverside.

Min, K.-E., Washenfelder, R., Dubé, W., Langford, A., Edwards, P., Zarzana, K., . . . Zhang, Y. (2016). A broadband cavity enhanced absorption spectrometer for aircraft measurements of glyoxal, methylglyoxal, nitrous acid, nitrogen dioxide, and water vapor. *Atmospheric Measurement Techniques*, 423-440.

Minato, A., Joarder, M. M. A., Ozawa, S., Kadoya, M., & Sugimoto, N. (1999). Development of a lidar system for measuring methane using a gas correlation method. *Japanese journal of applied physics, 38*(10R), 6130.

Mitchell, C., Sweet, J., & Jackson, T. (1990). A study of leakage from the UK natural gas distribution system. *Energy policy, 18*(9), 809-818.

Mokhatab, S., & Poe, W. A. (2012). *Handbook of natural gas transmission and processing*: Gulf professional publishing.

Molina, M. J., & Molina, L. T. (2004). Megacities and atmospheric pollution. *Journal of the Air & Waste Management Association, 54*(6), 644-680.

Naber, J., Siebers, D., Di Julio, S., & Westbrook, C. (1994). Effects of natural gas composition on ignition delay under diesel conditions. *Combustion and Flame, 99*(2), 192-200.

Nägele, M., & Sigrist, M. (2000). Mobile laser spectrometer with novel resonant multipass photoacoustic cell for trace-gas sensing. *Applied Physics B, 70*(6), 895-901.

Nilapwar, S. M., Nardelli, M., Westerhoff, H. V., & Verma, M. (2011). Absorption spectroscopy *Methods in enzymology* (Vol. 500, pp. 59-75): Elsevier.

O'Keefe, A., Scherer, J. J., & Paul, J. B. (1999). CW integrated cavity output spectroscopy. *Chemical Physics Letters, 307*(5-6), 343-349.

O'Keefe, A., & Deacon, D. A. (1988). Cavity ring-down optical spectrometer for absorption measurements using pulsed laser sources. *Review of scientific instruments, 59*(12), 2544-2551.

Olah, G. A. (2005). Beyond Oil and Gas: The Methanol Economy. *Angewandte Chemie International Edition, 44*(18), 2636-2639. doi:10.1002/anie.200462121

Orphal, J., & Ruth, A. A. (2008). High-resolution Fourier-transform cavity-enhanced absorption spectroscopy in the near-infrared using an incoherent broad-band light source. *Optics express, 16*(23), 19232-19243.

Osborn, S. G., Vengosh, A., Warner, N. R., & Jackson, R. B. (2011). Methane contamination of drinking water accompanying gas-well drilling and hydraulic fracturing. *Proceedings of the National Academy of Sciences, 108*(20), 8172-8176.

Pasquini, C. (2003). Near infrared spectroscopy: fundamentals, practical aspects and analytical applications. *Journal of the Brazilian Chemical Society, 14*(2), 198-219.

Paul, J. B., Lapson, L., & Anderson, J. G. (2001). Ultrasensitive absorption spectroscopy with a high-finesse optical cavity and off-axis alignment. *Applied Optics, 40*(27), 4904-4910.

Platt, U., & Stutz, J. (2008). Differential absorption spectroscopy *Differential Optical Absorption Spectroscopy* (pp. 135-174): Springer.

Press, W. H. (2007). *Numerical recipes 3rd edition: The art of scientific computing*: Cambridge university press.

Roarty, M. J., & Roarty, M. (2008). *Australia's natural gas: issues and trends*: Australia. Department of Parliamentary Services. Parliamentary Library.

Rodhe, H. (1990). A comparison of the contribution of various gases to the greenhouse effect. *Science, 248*(4960), 1217-1219.

Rohwedder, J. J. R., Pasquini, C., Fortes, P. R., Raimundo, I. M., Wilk, A., & Mizaikoff, B. (2014). iHWG-[small mu]NIR: a miniaturised near-infrared gas sensor based on substrate-integrated hollow waveguides coupled to a micro-NIR-spectrophotometer. *Analyst, 139*(14), 3572-3576. doi:10.1039/C4AN00556B

Romanini, D., Kachanov, A., Sadeghi, N., & Stoeckel, F. (1997). CW cavity ring down spectroscopy. *Chemical Physics Letters, 264*(3-4), 316-322.

Romanini, D., Ventrillard, I., Méjean, G., Morville, J., & Kerstel, E. (2014). Introduction to cavity enhanced absorption spectroscopy *Cavity-Enhanced Spectroscopy and Sensing* (pp. 1-60): Springer.

Ruth, A. A., Dixneuf, S., & Raghunandan, R. (2014). Broadband cavity-enhanced absorption spectroscopy with incoherent light *Cavity-Enhanced Spectroscopy and Sensing* (pp. 485-517): Springer.

Sawyer, R. F., Harley, R. A., Cadle, S., Norbeck, J., Slott, R., & Bravo, H. (2000). Mobile sources critical review: 1998 NARSTO assessment. *Atmospheric Environment, 34*(12), 2161-2181.

Schiff, H. I., Mackay, G. I., & Bechara, J. (1994). The use of tunable diode laser absorption spectroscopy for atmospheric measurements. *Research on Chemical Intermediates, 20*(3), 525-556. doi:10.1163/156856794x00441

Scott, S. L., & Barrufet, M. A. (2003). *Worldwide assessment of industry leak detection capabilities for single & multiphase pipelines*: Offshore Technology Research Center College Station.

Semin, R. A. B. (2008). A technical review of compressed natural gas as an alternative fuel for internal combustion engines. *American J. of Engineering and Applied Sciences, 1*(4), 302-311.

Shafiee, S., & Topal, E. (2009). When will fossil fuel reserves be diminished? *Energy policy, 37*(1), 181-189.

Siesler, H. W., Ozaki, Y., Kawata, S., & Heise, H. M. (2008). *Near-infrared spectroscopy: principles, instruments, applications*: John Wiley & Sons.

Sivathanu, Y. (2003). Technology status report on natural gas leak detection in pipelines. *Prepared for US Department of Energy, National Energy Technology Laboratory by Yudaya Sivathanu EnUrga Inc*.

Speight, J. G. (2007). *Natural gas: a basic handbook*: Elsevier.

Sperl, J. L. (1991). System pinpoints leaks on Point Arguello offshore line. *Oil and Gas Journal;(United States), 89*(36).

Thomas, S., & Dawe, R. A. (2003). Review of ways to transport natural gas energy from countries which do not need the gas for domestic use. *Energy, 28*(14), 1461-1477.

Thompson, G. M. (1991). Underground pipe leak detection system: Google Patents.

Triki, M., Cermak, P., Méjean, G., & Romanini, D. (2008). Cavity-enhanced absorption spectroscopy with a red LED source for NO x trace analysis. *Applied Physics B: Lasers and Optics, 91*(1), 195-201.

Turner, N. (1991). *Hardware and software techniques for pipeline integrity and leak detection monitoring.* Paper presented at the Offshore Europe.

Varma, R. M., Venables, D. S., Ruth, A. A., Heitmann, U., Schlosser, E., & Dixneuf, S. (2009). Long optical cavities for open-path monitoring of atmospheric trace gases and aerosol extinction. *Applied Optics, 48*(4), B159-B171. doi:10.1364/AO.48.00B159

Venables, D. (2016). Chapter 12 - Spectroscopic Measurement of Pollutant Gases. In M. de la Guardia & S. Armenta (Eds.), *Comprehensive Analytical Chemistry* (Vol. 73, pp. 295-319): Elsevier.

Venables, D. S., Gherman, T., Orphal, J., Wenger, J. C., & Ruth, A. A. (2006). High Sensitivity in Situ Monitoring of NO3 in an Atmospheric Simulation Chamber Using Incoherent Broadband Cavity-Enhanced Absorption Spectroscopy. *Environmental Science & Technology, 40*(21), 6758-6763. doi:10.1021/es061076j

Wang, M. Q., & Huang, H. S. (2000). *A full fuel-cycle analysis of energy and emissions impacts of transportation fuels produced from natural gas*. Retrieved from

Wang, Y., Xing, Z., Xu, H., & Du, K. (2016). Emission factors of air pollutants from CNG-gasoline bi-fuel vehicles: Part I. Black carbon. *Science of the total Environment, 572*, 1161-1165.

Washenfelder, R., Flores, J., Brock, C., Brown, S., & Rudich, Y. (2013). Broadband measurements of aerosol extinction in the ultraviolet spectral region. *Atmospheric Measurement Techniques, 6*(4), 861-877.

Washenfelder, R., Langford, A., Fuchs, H., & Brown, S. (2008). Measurement of glyoxal using an incoherent broadband cavity enhanced absorption spectrometer. *Atmospheric Chemistry and Physics, 8*(24), 7779-7793.

Weil, G. J. (1993). *Non contact, remote sensing of buried water pipeline leaks using infrared thermography.* Paper presented at the Water Management in the'90s: A Time for Innovation.

Werle, P., Mücke, R., & Slemr, F. (1993). The limits of signal averaging in atmospheric trace-gas monitoring by tunable diode-laser absorption spectroscopy (TDLAS). *Applied Physics B, 57*(2), 131-139.

Werle, P., Slemr, F., Maurer, K., Kormann, R., Mücke, R., & Jänker, B. (2002). Near-and mid-infrared laser-optical sensors for gas analysis. *Optics and lasers in engineering, 37*(2-3), 101-114.

White, J. U. (1976). Very long optical paths in air. *JOSA, 66*(5), 411-416.

Wu, T., Chen, W., Fertein, E., Cazier, F., Dewaele, D., & Gao, X. (2012). Development of an open-path incoherent broadband cavity-enhanced spectroscopy based instrument for simultaneous measurement of HONO and NO 2 in ambient air. *Applied Physics B, 106*(2), 501-509.

Wu, T., Coeur-Tourneur, C., Dhont, G., Cassez, A., Fertein, E., He, X., & Chen, W. (2014). Simultaneous monitoring of temporal profiles of NO 3, NO 2 and O 3 by incoherent broadband cavity enhanced absorption spectroscopy for atmospheric applications. *Journal of Quantitative Spectroscopy and Radiative Transfer, 133*, 199-205.

Wu, T., Zha, Q., Chen, W., Xu, Z., Wang, T., & He, X. (2014). Development and deployment of a cavity enhanced UV-LED spectrometer for measurements of atmospheric HONO and NO2 in Hong Kong. *Atmospheric Environment, 95*, 544-551.

Wu, T., Zhao, W., Chen, W., Zhang, W., & Gao, X. (2009). Incoherent broadband cavity enhanced absorption spectroscopy for in situ measurements of NO 2 with a blue light emitting diode. *Applied Physics B: Lasers and Optics, 94*(1), 85-94.

Yi, H., Wu, T., Wang, G., Zhao, W., Fertein, E., Coeur, C., . . . Chen, W. (2016). Sensing atmospheric reactive species using light emitting diode by incoherent broadband cavity enhanced absorption spectroscopy. *Optics express, 24*(10), A781-A790.

Zhang, J. (1997). Designing a cost-effective and reliable pipeline leak-detection system. *Pipes and Pipelines International, 42*(1), 20-26.

Zhao, W., Dong, M., Chen, W., Gu, X., Hu, C., Gao, X., . . . Zhang, W. (2013). Wavelength-resolved optical extinction measurements of aerosols using broad-band cavity-enhanced absorption spectroscopy over the spectral range of 445–480 nm. *Analytical chemistry, 85*(4), 2260-2268.

Appendix

NIR-IBBCEAS Mirror Reflectivity

Wavelength (nm)	R (λ)
1105.35	0.998321
1106.79	0.998327
1108.22	0.998333
1109.65	0.99834
1111.09	0.998346
1112.52	0.998352
1113.95	0.998359
1115.38	0.998365
1116.81	0.998371
1118.24	0.998378
1119.66	0.998384
1121.09	0.99839
1122.52	0.998396
1123.94	0.998403
1125.36	0.998409
1126.79	0.998415
1128.21	0.998421
1129.63	0.998426
1131.05	0.998431

1132.47	0.998436
1133.89	0.998442
1135.31	0.998447
1136.73	0.998452
1138.14	0.998458
1139.56	0.998463
1140.97	0.998468
1142.39	0.998474
1143.8	0.998479
1145.21	0.998484
1146.63	0.998488
1148.04	0.998493
1149.45	0.998497
1150.85	0.998501
1152.26	0.998505
1153.67	0.998509
1155.08	0.998513
1156.48	0.998516
1157.89	0.99852
1159.29	0.998523
1160.69	0.998526
1162.1	0.998529

1163.5	0.998532
1164.9	0.998535
1166.3	0.998537
1167.7	0.99854
1169.1	0.998543
1170.49	0.998546
1171.89	0.998548
1173.28	0.99855
1174.68	0.998552
1176.07	0.998554
1177.47	0.998556
1178.86	0.998558
1180.25	0.99856
1181.64	0.998561
1183.03	0.998563
1184.42	0.998564
1185.81	0.998565
1187.19	0.998566
1188.58	0.998567
1189.97	0.998568
1191.35	0.998569
1192.73	0.998569

1194.12	0.998568
1195.5	0.998567
1196.88	0.998566
1198.26	0.998565
1199.64	0.998564
1201.02	0.998563
1202.4	0.998562
1203.77	0.998561
1205.15	0.99856
1206.53	0.998559
1207.9	0.998558
1209.27	0.998557
1210.65	0.998556
1212.02	0.998555
1213.39	0.998554
1214.76	0.998553
1216.13	0.998552
1217.5	0.998551
1218.87	0.99855
1220.23	0.998549
1221.6	0.998548
1222.97	0.998547

1224.33	0.998546
1225.69	0.998545
1227.06	0.998544
1228.42	0.998543
1229.78	0.998542
1231.14	0.998541
1232.5	0.998538
1233.86	0.998535
1235.22	0.998533
1236.57	0.99853
1237.93	0.998528
1239.28	0.998525
1240.64	0.998522
1241.99	0.99852
1243.34	0.998517
1244.7	0.998515
1246.05	0.998512
1247.4	0.998509
1248.75	0.998507
1250.1	0.998504

Absorption cross-section

Methane

Wavelength (nm)	σ ($cm^2 molecule^{-1}$)
1105.35	1.19E-24
1106.79	1.71E-24
1108.22	2.37E-24
1109.65	3.51E-24
1111.09	4.38E-24
1112.52	5.63E-24
1113.95	6.78E-24
1115.38	7.85E-24
1116.81	9.31E-24
1118.24	1.26E-23
1119.66	1.69E-23
1121.09	2.17E-23
1122.52	2.61E-23
1123.94	3.07E-23
1125.36	3.37E-23
1126.79	3.42E-23
1128.21	3.25E-23
1129.63	3.06E-23
1131.05	3.33E-23

1132.47	3.51E-23
1133.89	3.55E-23
1135.31	3.52E-23
1136.73	3.42E-23
1138.14	3.13E-23
1139.56	2.82E-23
1140.97	2.29E-23
1142.39	2.16E-23
1143.8	2.32E-23
1145.21	2.64E-23
1146.63	3.09E-23
1148.04	3.82E-23
1149.45	4.84E-23
1150.85	6.00E-23
1152.26	7.12E-23
1153.67	7.78E-23
1155.08	7.91E-23
1156.48	7.87E-23
1157.89	8.14E-23
1159.29	8.15E-23
1160.69	8.36E-23
1162.1	8.40E-23

1163.5	8.48E-23
1164.9	8.31E-23
1166.3	7.73E-23
1167.7	6.67E-23
1169.1	5.77E-23
1170.49	5.13E-23
1171.89	4.66E-23
1173.28	4.23E-23
1174.68	3.78E-23
1176.07	3.39E-23
1177.47	3.08E-23
1178.86	2.83E-23
1180.25	2.59E-23
1181.64	2.38E-23
1183.03	2.24E-23
1184.42	2.17E-23
1185.81	2.06E-23
1187.19	2.00E-23
1188.58	1.87E-23
1189.97	1.74E-23
1191.35	1.57E-23
1192.73	1.35E-23

1194.12	1.12E-23
1195.5	9.70E-24
1196.88	8.36E-24
1198.26	7.32E-24
1199.64	6.54E-24
1201.02	5.90E-24
1202.4	5.17E-24
1203.77	4.56E-24
1205.15	3.87E-24
1206.53	3.22E-24
1207.9	2.63E-24
1209.27	2.15E-24
1210.65	1.73E-24
1212.02	1.45E-24
1213.39	1.21E-24
1214.76	1.01E-24
1216.13	8.17E-25
1217.5	6.68E-25
1218.87	4.96E-25
1220.23	4.37E-25
1221.6	3.91E-25
1222.97	3.47E-25

1224.33	3.76E-25
1225.69	4.23E-25
1227.06	4.64E-25
1228.42	4.93E-25
1229.78	5.26E-25
1231.14	5.52E-25
1232.5	5.45E-25
1233.86	5.02E-25
1235.22	4.33E-25
1236.57	3.65E-25
1237.93	3.13E-25
1239.28	2.64E-25
1240.64	1.93E-25
1241.99	1.71E-25
1243.34	1.48E-25
1244.7	1.32E-25
1246.05	1.04E-25
1247.4	8.12E-26
1248.75	6.28E-26
1250.1	3.83E-26

Butane

Wavelength (nm)	σ ($cm^2 molecule^{-1}$)
1105.35	1.61E-23
1106.79	1.61E-23
1108.22	1.62E-23
1109.65	1.62E-23
1111.09	1.64E-23
1112.52	1.65E-23
1113.95	1.67E-23
1115.38	1.69E-23
1116.81	1.72E-23
1118.24	1.75E-23
1119.66	1.79E-23
1121.09	1.84E-23
1122.52	1.90E-23
1123.94	1.98E-23
1125.36	2.06E-23
1126.79	2.17E-23
1128.21	2.29E-23
1129.63	2.42E-23
1131.05	2.58E-23
1132.47	2.75E-23

1133.89	2.95E-23
1135.31	3.16E-23
1136.73	3.40E-23
1138.14	3.65E-23
1139.56	3.93E-23
1140.97	4.22E-23
1142.39	4.52E-23
1143.8	4.83E-23
1145.21	5.16E-23
1146.63	5.48E-23
1148.04	5.81E-23
1149.45	6.13E-23
1150.85	6.44E-23
1152.26	6.74E-23
1153.67	7.03E-23
1155.08	7.30E-23
1156.48	7.56E-23
1157.89	7.80E-23
1159.29	8.03E-23
1160.69	8.24E-23
1162.1	8.46E-23
1163.5	8.67E-23

1164.9	8.88E-23
1166.3	9.12E-23
1167.7	9.38E-23
1169.1	9.68E-23
1170.49	1.00E-22
1171.89	1.05E-22
1173.28	1.11E-22
1174.68	1.20E-22
1176.07	1.32E-22
1177.47	1.50E-22
1178.86	1.73E-22
1180.25	2.00E-22
1181.64	2.28E-22
1183.03	2.52E-22
1184.42	2.69E-22
1185.81	2.76E-22
1187.19	2.73E-22
1188.58	2.63E-22
1189.97	2.51E-22
1191.35	2.41E-22
1192.73	2.33E-22
1194.12	2.30E-22

1195.5	2.28E-22
1196.88	2.28E-22
1198.26	2.28E-22
1199.64	2.27E-22
1201.02	2.24E-22
1202.4	2.20E-22
1203.77	2.15E-22
1205.15	2.08E-22
1206.53	2.00E-22
1207.9	1.91E-22
1209.27	1.81E-22
1210.65	1.71E-22
1212.02	1.59E-22
1213.39	1.48E-22
1214.76	1.37E-22
1216.13	1.25E-22
1217.5	1.14E-22
1218.87	1.03E-22
1220.23	9.32E-23
1221.6	8.37E-23
1222.97	7.48E-23
1224.33	6.67E-23

1225.69	5.94E-23
1227.06	5.28E-23
1228.42	4.70E-23
1229.78	4.19E-23
1231.14	3.74E-23
1232.5	3.36E-23
1233.86	3.03E-23
1235.22	2.76E-23
1236.57	2.53E-23
1237.93	2.34E-23
1239.28	2.18E-23
1240.64	2.05E-23
1241.99	1.95E-23
1243.34	1.87E-23
1244.7	1.80E-23
1246.05	1.75E-23
1247.4	1.71E-23
1248.75	1.68E-23
1250.1	1.66E-23

Ethane

Wavelength (nm)	σ ($cm^2molecule^{-1}$)
1105.35	3.30E-23
1106.79	3.30E-23
1108.22	3.30E-23
1109.65	3.31E-23
1111.09	3.31E-23
1112.52	3.31E-23
1113.95	3.32E-23
1115.38	3.33E-23
1116.81	3.34E-23
1118.24	3.36E-23
1119.66	3.40E-23
1121.09	3.45E-23
1122.52	3.52E-23
1123.94	3.61E-23
1125.36	3.74E-23
1126.79	3.90E-23
1128.21	4.10E-23
1129.63	4.34E-23
1131.05	4.62E-23
1132.47	4.92E-23

1133.89	5.25E-23
1135.31	5.58E-23
1136.73	5.89E-23
1138.14	6.17E-23
1139.56	6.41E-23
1140.97	6.58E-23
1142.39	6.68E-23
1143.8	6.71E-23
1145.21	6.67E-23
1146.63	6.58E-23
1148.04	6.45E-23
1149.45	6.32E-23
1150.85	6.21E-23
1152.26	6.15E-23
1153.67	6.17E-23
1155.08	6.29E-23
1156.48	6.55E-23
1157.89	6.95E-23
1159.29	7.50E-23
1160.69	8.20E-23
1162.1	9.07E-23
1163.5	1.01E-22

1164.9	1.12E-22
1166.3	1.25E-22
1167.7	1.38E-22
1169.1	1.52E-22
1170.49	1.65E-22
1171.89	1.78E-22
1173.28	1.90E-22
1174.68	2.01E-22
1176.07	2.10E-22
1177.47	2.17E-22
1178.86	2.22E-22
1180.25	2.23E-22
1181.64	2.23E-22
1183.03	2.19E-22
1184.42	2.13E-22
1185.81	2.05E-22
1187.19	1.94E-22
1188.58	1.83E-22
1189.97	1.70E-22
1191.35	1.56E-22
1192.73	1.43E-22
1194.12	1.29E-22

1195.5	1.16E-22
1196.88	1.04E-22
1198.26	9.24E-23
1199.64	8.22E-23
1201.02	7.32E-23
1202.4	6.54E-23
1203.77	5.88E-23
1205.15	5.32E-23
1206.53	4.86E-23
1207.9	4.49E-23
1209.27	4.20E-23
1210.65	3.97E-23
1212.02	3.79E-23
1213.39	3.65E-23
1214.76	3.55E-23
1216.13	3.48E-23
1217.5	3.42E-23
1218.87	3.39E-23
1220.23	3.36E-23
1221.6	3.34E-23
1222.97	3.33E-23
1224.33	3.32E-23

1225.69	3.31E-23
1227.06	3.31E-23
1228.42	3.31E-23
1229.78	3.31E-23
1231.14	3.30E-23
1232.5	3.30E-23
1233.86	3.30E-23
1235.22	3.30E-23
1236.57	3.30E-23
1237.93	3.30E-23
1239.28	3.30E-23
1240.64	3.30E-23
1241.99	3.30E-23
1243.34	3.30E-23
1244.7	3.30E-23
1246.05	3.30E-23
1247.4	3.30E-23
1248.75	3.30E-23
1250.1	3.30E-23

Propane

Wavelength (nm)	σ ($cm^2 molecule^{-1}$)
1105.35	1.45E-23
1106.79	1.45E-23
1108.22	1.45E-23
1109.65	1.45E-23
1111.09	1.45E-23
1112.52	1.45E-23
1113.95	1.45E-23
1115.38	1.46E-23
1116.81	1.47E-23
1118.24	1.48E-23
1119.66	1.50E-23
1121.09	1.52E-23
1122.52	1.56E-23
1123.94	1.61E-23
1125.36	1.69E-23
1126.79	1.79E-23
1128.21	1.91E-23
1129.63	2.08E-23
1131.05	2.28E-23
1132.47	2.52E-23

1133.89	2.81E-23
1135.31	3.15E-23
1136.73	3.52E-23
1138.14	3.93E-23
1139.56	4.36E-23
1140.97	4.79E-23
1142.39	5.22E-23
1143.8	5.63E-23
1145.21	5.99E-23
1146.63	6.30E-23
1148.04	6.54E-23
1149.45	6.71E-23
1150.85	6.80E-23
1152.26	6.83E-23
1153.67	6.79E-23
1155.08	6.72E-23
1156.48	6.64E-23
1157.89	6.56E-23
1159.29	6.52E-23
1160.69	6.54E-23
1162.1	6.66E-23
1163.5	6.88E-23

1164.9	7.23E-23
1166.3	7.71E-23
1167.7	8.33E-23
1169.1	9.09E-23
1170.49	9.98E-23
1171.89	1.10E-22
1173.28	1.21E-22
1174.68	1.33E-22
1176.07	1.45E-22
1177.47	1.57E-22
1178.86	1.70E-22
1180.25	1.81E-22
1181.64	1.92E-22
1183.03	2.02E-22
1184.42	2.11E-22
1185.81	2.17E-22
1187.19	2.22E-22
1188.58	2.25E-22
1189.97	2.26E-22
1191.35	2.24E-22
1192.73	2.21E-22
1194.12	2.15E-22

1195.5	2.08E-22
1196.88	1.99E-22
1198.26	1.89E-22
1199.64	1.77E-22
1201.02	1.65E-22
1202.4	1.52E-22
1203.77	1.40E-22
1205.15	1.27E-22
1206.53	1.14E-22
1207.9	1.02E-22
1209.27	9.12E-23
1210.65	8.06E-23
1212.02	7.10E-23
1213.39	6.23E-23
1214.76	5.45E-23
1216.13	4.77E-23
1217.5	4.17E-23
1218.87	3.66E-23
1220.23	3.23E-23
1221.6	2.87E-23
1222.97	2.57E-23
1224.33	2.33E-23

1225.69	2.13E-23
1227.06	1.97E-23
1228.42	1.84E-23
1229.78	1.75E-23
1231.14	1.67E-23
1232.5	1.61E-23
1233.86	1.57E-23
1235.22	1.53E-23
1236.57	1.51E-23
1237.93	1.49E-23
1239.28	1.48E-23
1240.64	1.47E-23
1241.99	1.46E-23
1243.34	1.46E-23
1244.7	1.45E-23
1246.05	1.45E-23
1247.4	1.45E-23
1248.75	1.45E-23
1250.1	1.45E-23

Platform Design for Light Source Integration

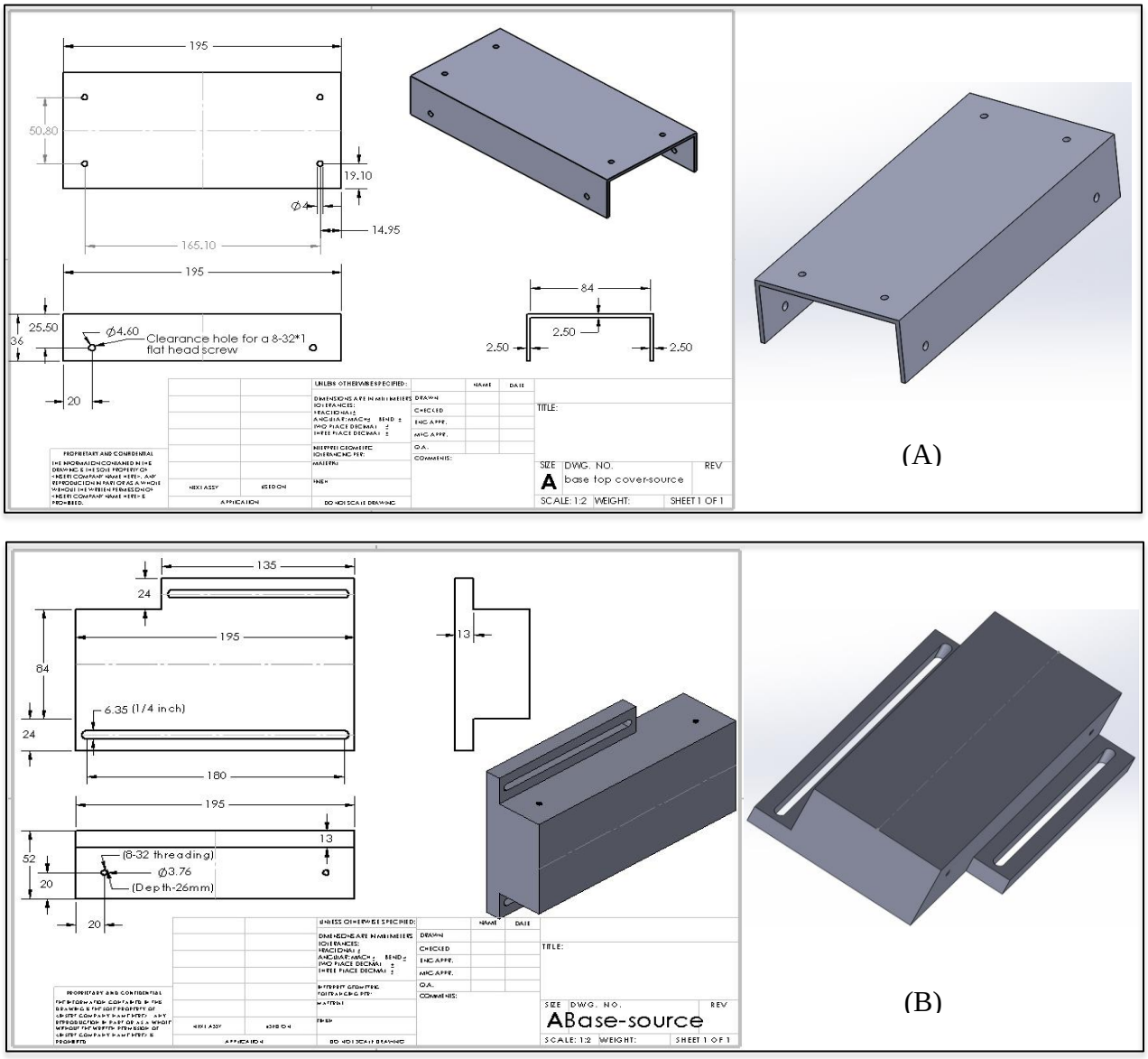

Figure 26: The platform designed to place the tungsten-halogen lamp (bulb and focusing optics) dismantled from the original source box. It constitutes a top cover (A) and a base (B) where the former is attached over the latter by screwing them together. The lamp is fixed over the top cover while the base is attached to the breadboard. The dimensions are decided such that the center of bulb is at the required optical height.